Final Report
(CSM Project 4-42857)

Phase IV
Enhanced Shielded Metal Arc Electrode Development for Underwater Wet Welding: Technology Transfer to Industry

Submitted to:
Mr. Michael Else
Minerals Management Service
Engineering and Research Branch
382 Elden St. Herndon, VA 20170

Prepared by:
Luciano Andrade, Dr. Stephen Liu, and Dr. Faustino Perez
Center for Welding, Joining and Coatings Research
Colorado School of Mines
Golden, Colorado 80401
CSM Report #: MT-CWJCR-009-001

Research Performed Under Contract:
M08PX20049/0010000447

March 2009

TABLE OF CONTENTS

SUMMARY 1

1. INTRODUCTION 2
1.1. Objectives of this research 4
1.2. Research Personnel 4

2. EXPERIMENTAL RUTILE BASE ELECTRODES 4

3. EXPERIMENTAL PROCEDURES 5
3.1. Electrode Extrusion 5
3.2. BOP and Multipass V-Groove Welds 6

4. RESULTS 11
4.1. Wet welds made using "wet 1" electrodes extruded at CSM 11
4.1.1. Porosity of wet welds 11
4.1.2. Bead-on-Plate Wet Welds 13
4.1.3. V-Groove Wet Welds 22
4.2. Wet welds made using "wet 1" electrodes extruded at Devasco 25

5. CONCLUSIONS AND RECOMMENDATIONS 29
5.1. Conclusions 30
5.2. Further Considerations of the Results 30
5.3. Recommendations 31

6. ACKNOWLEDGMENTS 31

7. REFERENCES 31

APPENDIX A: The Gravimetric Method for Porosity Quantification 33
A.1. Porosity calculation for zero weld penetration 34
A.2. Porosity calculation for deeper weld penetration 35

APPENDIX B: Particle Size Distribution of the Minerals used in Extrusion 38

List of Tables

Table 1. Flux formulations. 5

Table 2. Experimental matrix of “wet 1” extruded at CSM, used during initial tests. 8

Table 3. Selected parameters for “wet 1” electrodes extruded at CSM. 8

Table 4. Experimental matrix of “wet 1” extruded at CSM, using DCEN at 328 ft. 9

Table 5. Experimental matrix of “wet 1” extruded at Devasco, International, at 1 ft. 9

Table 6. Experimental matrix of “wet 1” extruded at Devasco, International, at 200 ft. 10

Table 7. Porosity quantification. “wet 1” electrodes extruded at CSM. 13

Table 8. Summary of the weld parameters. 16

Table 9. Weld bead morphology values. 17

Table 10. Chemical analyses made on weld metal. 20

Table B1. Relation between the mesh number used and the size of the mesh. 38

List of Figures

Figure 1. Blender used for flux mixing. 6

Figure 2. Electrode extruder. 6

Figure 3. Steel plate arrangement for V-groove wet welds. 7

Figure 4. Hyperbaric chamber (a) used to perform the wet welds with the gravity welder (b) placed inside the chamber. The angle α between the electrode and base plate is also defined. 7

Figure 5. Schematic drawing showing the spots analyzed for microstructure. 11

Figure 6. Schematic showing the location of the indentations. 11

Figure 7. Schematic drawing showing the steps of sample preparation for chemical analysis. 11

Figure 8. weld made using "wet 1" electrodes extruded at CSM. 12

Figure 9. Weld bead macro-photograph extracted from the middle section of the welds. 13

Figure 10. Wet welds made at 100 ft. using "wet 1" electrodes extruded at CSM. 14

Figure 11. Wet welds made at 200 ft. using "wet 1" electrodes extruded at CSM. 14

Figure 12. Wet welds made at 328 ft. using "wet 1" electrodes extruded at CSM. 14

Figure 13. Arc voltage signal from the BOP wet weld made at 100 ft. 15

Figure 14. Arc voltage signal from the BOP wet weld made at 200 ft. 15

Figure 15. Arc voltage signal from the BOP wet weld made at 328 ft. 16

Figure 16. Weld bead microstructure. 18

Figure 17. Weld bead microstructure quantification. 18

Figure 18. Weld bead microphotographs from fusion line illustrating epitaxial growth. 19

Figure 19. Micro hardness measured on line 1. 19

Figure 20. Micro hardness measured on line 2. 20

Figure 21. Weld metal chemical composition variation with water depth. 21

Figure 22. Weld metal manganese concentration compared with prior works (M. Rowe, 1999; F. Guerrero, 2003). 21

Figure 23. Weld metal silicon concentration compared with prior works (M. Rowe, 1999; F. Guerrero, 2003). 22

Figure 24. Different bead quality obtained at 328 ft. using selected electrodes after extrusion. A – Poor quality along all bead length; B – Poor quality in the beginning of the bead, but good quality at the end of the bead; C – Good quality along all bead length.
Scale in millimeters. 23

Figure 25. First steel plate arrangement used for V-groove wet welds. 23

Figure 26. V-groove radiographic films. A – 100ft.; B – 200 ft.; C – 328ft. 24

Figure 27. Typical voltage signal acquired during V-groove wet welding at 100 ft. 24

Figure 28. Typical voltage signal acquired during V-groove wet welding at 200 ft. 25

Figure 29. Typical voltage signal acquired during V-groove wet welding at 328 ft. 25

Figure 30. Typical weld produced using "wet1" extruded at Devasco, International, at 1 ft. water depth. 26

Figure 31. Typical voltage signals from welds made at 1 ft. water depth, using "wet 1" electrodes extruded at Devasco, International. 26

Figure 32. The best weld made at 200 ft. using an angle of 45°. 28

Figure 33. The best weld made at 200 ft. using an angle of 47°. 28

Figure 34. The best weld made at 200 ft. using an angle of 50°. 28

Figure 35. Typical voltage signals from welds made at 200 ft. water depth,
using "wet 1" electrodes extruded at Devasco, International. 29

Figure A.1. Weld with no penetration. 34

Figure A.2. Weld with deeper penetration. 35

Figure A3. Base metal preparation. 36

Figure A4. Equipment used to weigh suspended sample. 36

Figure A5. Device used to measure the wet weight. 37

Figure B1. Particle size comparison of TiO_2 between CSM and Devasco Fluxes. 38

Figure B2. Particle size comparison of feldspar between CSM and Devasco Fluxes. 39

Figure B3. Particle size comparison of mica between CSM and Devasco Fluxes. 39

Figure B4. Particle size comparison of silica between CSM and Devasco Fluxes. 40

Figure B5. Particle size comparison of kaolin between CSM and Devasco Fluxes. 40

Figure B6. Particle size comparison of iron between CSM and Devasco Fluxes. 41

Figure B7. Particle size comparison of marflux between CSM and Devasco Fluxes. 41

Figure B8. Particle size comparison of ZrO_2 between CSM and Devasco Fluxes. 42

Figure B9. Particle size comparison of Fe-Mn between CSM and Devasco Fluxes. 42

Figure B10. Particle size comparison of Fe-Ti between CSM and Devasco Fluxes. 43

Figure B11. Particle size comparison of Fe-B between CSM and Devasco Fluxes. 43

SUMMARY

This report presents the results obtained in the research work carried out in Phase IV of the underwater wet welding program sponsored by the Minerals Management Service (MMS) of the U.S. Department of the Interior.

Experimental rutile-grade electrodes were produced for underwater wet welding. Alloying elements were added to the flux coating for the purpose of controlling the loss of elements by oxidation, and extruded onto core rods that contained very low carbon content to minimize weld porosity. One flux formula was selected out of three formulations defined in the last phase of this program for the work described in this report.

Bead-on-plate (BOP) wet welds were made with the experimental electrode. Arc stability, slag detachability, and bead morphology were examined during welding. Arc voltage and current signals were collected during all welds for metal transfer mode and stability analysis. Cross sections extracted from the welds were used to analyze the macro and microstructure present and to make hardness measurements. Porosity was determined separately, using the gravimetric method, as described in Appendix A.

Core rods that contained 0.001 wt. pct. carbon were used to make the electrodes. With these electrodes, welds obtained at 200 ft. (61 m) water depth averaged 1.46 pct. porosity and exhibited good bead morphology. Higher recovery of manganese and silicon was observed in the current welds than previous phases of the project.

Based on the current results and conclusions, the next step of this electrode development program for wet welding should match the technology used by the industry, conducting minor tune-up of the electrodes for volume production and to transfer the technology to industry. Inability to match the exact compositions will unfortunately delay the final testing of these innovative electrodes to a future testing and qualification phase that is being organized at the time of this report.

1. INTRODUCTION

It is well known that in underwater wet welding of structural steels, the wet environment poses some major challenges as listed below:

- Loss of alloying elements, caused by the oxidizing environment;
- Increase in porosity, caused by the formation of CO in the droplet;
- Increase in arc instability, caused by the ambient pressure;
- Increase in amount and size of non-metallic inclusions;
- Coarsening of microstructure, caused by the loss of alloying elements;
- Formation of martensite and bainite in the heat affected zone, caused by the high cooling rate;
- Incidence of cracks, caused by high hydrogen concentration, high cooling rate and consequently high hardness in the heat affected zone; and
- Deterioration of mechanical properties, cause by all of these problems described above.

To compensate for the effect of these problems, underwater wet welding requires higher quality consumables. Several research projects were conducted at CSM to optimize shielded metal arc welding consumables (stick electrodes) for underwater wet welding.

Sanchez, Liu et al. (1994) studied the effect of calcium carbonate ($CaCO_3$) addition in the electrode flux of E6013 type electrodes. He concluded that calcium carbonate additions of up to 12.5 wt. pct. resulted in reduction of weld metal porosity. Above this concentration, deterioration in arc stability and slag detachability occurred. Calcium carbonate is a gas former, and decomposes according to Equations 1 and 2.

$$CaCO_{3(s)} \Rightarrow CaO_{(s)} + CO_{2(g)} \qquad \text{Eq. 1}$$

$$CO_2 + C \Leftrightarrow 2CO \qquad \text{Eq. 2}$$

The CO gas produced from the decomposition of CO_2 reduces the partial pressure of hydrogen in the arc, which will decrease hydrogen pick-up in the weld metal and decrease the porosity formed by hydrogen in the weld metal.

Pope, Liu et al. (1995) investigated the influence of nickel additions on the tensile strength and impact resistance of wet welds made at 1.1 m of water depth. Using additions of nickel in the flux covering and/or in the steel core rod of oxidizing electrodes, qualified welder/divers deposited V-groove wet welds on low carbon steel plates to extract standard Charpy v-notch specimens and reduced-size tensile specimens for mechanical tests. He found that Charpy v-notch impact energy and the tensile strength presented maximum values between 2 and 3 wt. pct. of nickel in the weld metal. Further increases in nickel content lowered the toughness and the tensile strength, caused by the presence of solidification cracks in the weld metal. They also concluded that nickel additions had a significant effect in reducing the grain size of equiaxed ferrite in the reheated region of multipass wet welds.

The improvement of the toughness of ferritic iron alloys promoted by nickel additions is usually explained by the ability of this element in facilitating cross slip of screw dislocations,

thereby reducing local stress concentrations capable of initiating cleavage (Floreen et al., 1971). It seems, however, that part of the improvement on the impact resistance of the weld must be attributed to the grain size refinement promoted by nickel.

Medeiros and Liu (1998) reported significant reduction of diffusible hydrogen from 50 to 13 ml/100g by increasing the hematite in the flux of oxidizing electrodes from 0 to 53 wt. pct. Hematite decomposes to form FeO in the slag, thus increasing slag basicity (according to Tuliani's basicity index formula, Equation 3). They noted a similar trend for total hydrogen (diffusible and residual). If porosity in wet welds is caused by hydrogen and weld metal hydrogen is affected by slag basicity, it can be expected that slag basicity will affect the amount of porosity in underwater wet welds.

$$B.I. = \frac{CaF_2 + CaO + MgO + BaO + SrO + K_2O + Na_2O + \frac{1}{2}\left(FeO + MnO\right)}{SiO_2 + \frac{1}{2}\left(Al_2O_3 + TiO_2 + ZrO_2\right)} \qquad \text{Eq. 3}$$

To verify the contribution of CO in wet weld porosity, Rowe and Liu (1999) studied the effect of Fe-Mn and Fe-Ti additions in the electrode flux. Titanium and manganese are strong deoxidizers that react with oxygen in the weld pool, consequently decreasing the amount of CO formed in the molten metal and decreasing porosity. They found that the porosity decreased with increasing ferro-manganese addition. Manganese and titanium additions were able to reduce porosity from approximately 8 vol. pct. to around 1 vol. pct.

Another way to decrease the CO formation in the molten metal is decreasing the amount of carbon in the system. Liu and Perez (2007) concluded that the porosity in the weld metal can be reduced using electrodes produced with core rods with low carbon content.

Rowe and Liu (1999) also concluded that additions of titanium and boron were effective in refining the ferrite grain size of the as-deposited and reheated microstructures of steel wet weld. With the combined additions of titanium, boron and manganese, the microstructures of structural steel wet welds were optimized to contain high amounts (greater than 70 vol. pct.) of acicular ferrite. Rare earth metals (REM) were also investigated but showed no definitive effects.

Perez and Liu (2003) studied the effect of nickel additions to rutile-grade electrodes for underwater wet welding. He concluded that small amounts of nickel, 2.3 wt. pct., improve the impact toughness of the wet welds, and the toughness improvements are associated to the ferrite grain refinement observed.

Some arc stabilizers can be added in the electrode flux to increase the arc stability, and produce better welds with lower porosity. The weld parameters affect directly the weld porosity. Perez (2007) and Liu and Perez (2004) found that the globular transfer mode produced welds with lower porosity than welds made with short-circuiting. Bracarense et al. (2003) and Liu and Perez (2004) concluded that, using rutile-grade electrodes, direct current electrode positive (DCEP) produced less porosity in wet welds.

Perez (2007) proposed a mechanism of porosity formation in underwater wet welding. He concluded that the porosity in wet weld was produced by CO gas that formed, trapped and transported in the droplet. Upon detachment, the gas bubble would be incorporated into the weld. Porosity can thus be minimized using electrodes with low carbon steel rods and deoxidizer additions in the covering. He also concluded that the metal transfer modes have a strong relationship with weld metal porosity. Short-circuiting transfer promotes the formation of larger

droplets that will transport more gas than the fine droplets associated with spray or globular transfer.

Pessoa, Liu et al. (2007) studied the influence of exothermic additions in a tubular covered E6013 grade electrode. By adding aluminum and calcium carbide inside the tubular core rod, they concluded that the addition of these two ingredients reduced porosity formation through decreasing CO and the droplet size, while promoted acicular ferrite formation and increased the recovery of alloying elements.

Based on these results, the investigators proposed an electrode formulation that combined the beneficial effects from the previous studies that contained optimized amounts of Fe-Ti-Mn-REM and Fe-Mn additions to produce welds with enhanced weld metal microstructures and properties.

1.1. Objective of this Research

The main objective of Phase IV of this program is to develop a commercially viable shielded metal arc welding electrode and transfer the product to the wet welding industry.

1.2. Research Personnel

This research program was conducted at the Colorado School of Mines by Mr. Luciano Andrade and Prof. Stephen Liu. Dr. Faustino Perez-Guerrero at the Instituto Mexicano del Petróleo and Dr. Ezequiel Pessoa at the Universidade Federal de Minas Gerais worked on the initial phases of this program. Dr. Faustino Perez-Guerrero also contributed to this report. Prof. Alex Bracarense at the Universidade Federal de Minas Gerais has been an invaluable partner in the CSM underwater wet welding program for the last decade.

2. EXPERIMENTAL RUTILE BASE ELECTRODES

Since rutile-grade electrodes have exhibited good results in wet welding, this slightly basic flux formulation was used to extrude shielded metal arc welding electrodes for this experimental program using a “carbon-free” steel core rod, with merely 0.001 wt. pct. carbon. Only one out of the three flux formulae investigated and designed in previous phases of this project was selected for the extrusion of experimental electrodes for wet welding.

Table 1 presents the optimized flux formulations from previous studies as well as the formulations selected for extrusion in this phase of work. F64[a] and F65[b] are from Perez-Guerrero’s work in 2007. The electrodes F64[a] and F65[b] were extruded using steel rods that contained 0.059 wt. pct. carbon and 0.005 wt. pct. carbon, respectively.

“Wet 1” and “wet 2” are the formulations used in this work. In particular, formula “wet 1” was modified according to the experimental welding results to develop electrode “wet 2”. The Fe-Mn, Fe-Ti and Ni additions were made in formula “wet 2” to achieve the desire weld metal composition, considering results from welds made using “wet 1” electrodesand bead-on-plate (BOP) welding. Additionally, the “wet 1” electrodes were extruded at the Colorado School of Mines. Devasco, International also extruded electrodes using formula “wet 1”, which were used subsequently to produce V-groove welds. Formula “wet 2” was produced only by Devasco,

International for bead-on-plate welding and V-groove welding. In the electrodes produced by Devasco, International, kaolin ($Al_2O_3.2SiO_2.2H_2O$) was replaced by bentonite, a complex Al, Mg, Ca, and Fe hydroxide. Both electrodes "wet 1" and "wet 2" were extruded using a steel rod with 0.001 wt. pct. carbon. The rods had 4 mm (5/32 in.) diameter and were 356 mm (14 in.) long.

Table 1. Flux formulations.

** - Kaolin was replaced by bentonite on electrodes produced by Devasco, International.

Minerals	Function	F64[a], F65[b]	Wet 1	Wet 2
TiO2	Arc stabilizer; Slag former	41.8	41.8	39.0
Feldspar	Slag former; Arc stabilizer	31.2	31.2	28.5
Mica	Slipping agent			
Silica	Slag former			
Kaolin**	Slipping agent			
Reduced Iron	Arc stabilizer			
Marflux (CaCO3)	Gas former			
ZrO2	Arc stabilizer			
Fe-Mn	Deoxidizer; Alloying agent	16	16	18
Fe-Ti	Alloying agent; Deoxidizer	5	5	7,5
Fe-B	Alloying agent	1	1	1
Ni	Alloying agent	4.8	4.8	5.8
CMC	Slipping agent	-	0.2	0.2

3. EXPERIMENTAL PROCEDURES

3.1. Electrode Extrusion

The experimental electrodes "wet 1" were extruded at CSM using the pilot scale production facilities available. Figure 1 and 2 shows photographs of the blender used for mixing the flux ingredients and the electrode extruder. Following extrusion, the electrodes were dried at room temperature for 24 hours and baked at 300° F for 90 minutes. Only the electrodes that showed uniform flux thickness and concentricity were selected for waterproofing with a layer of polyurethane-base commercial varnish to protect the flux coating from water absorption during welding. The core rod used had 4.0 mm and the total diameter of the electrodes including flux was 5.7 mm. ASTM A-36 grade carbon steel plates were used for all tests.

Figure 1. Blender used for flux mixing.

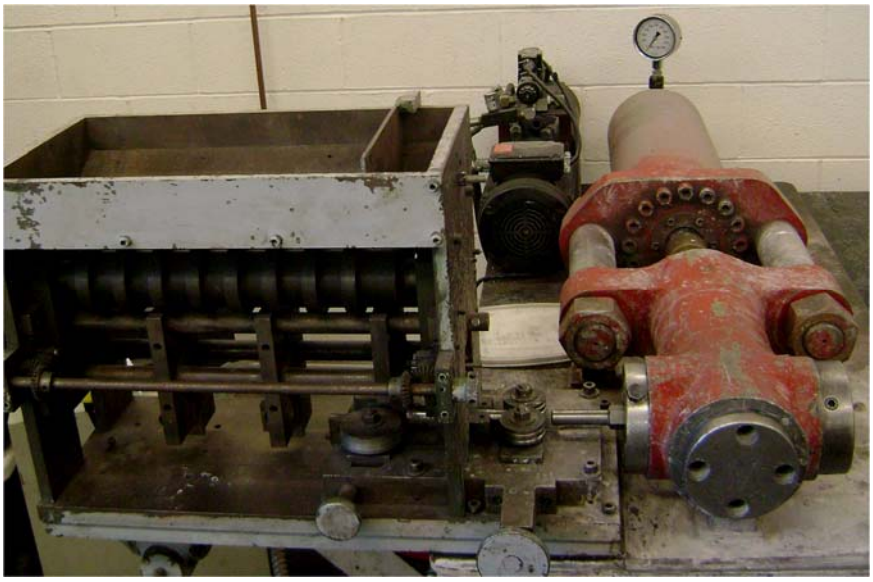

Figure 2. Electrode extruder.

3.2. BOP and Multipass V-Groove Welds

Both bead-on-plate (BOP) and multipass V-groove wet welds were produced in this phase of the project. BOP wet welds are usually considered necessary for the identification of appropriate welding parameters for the experimental electrodes. Transverse cross-sections extracted from the BOP welds are typically used for macro- and micro-structural characterization, chemical analysis, hardness measurement, porosity, and the quantification of other defects. On the other hand, V-groove wet welds are also necessary for extracting specimens

for mechanical testing. Multipass V-groove wet welds were deposited on 200 mm long ASTM A-36 steel plates according to Figure 3.

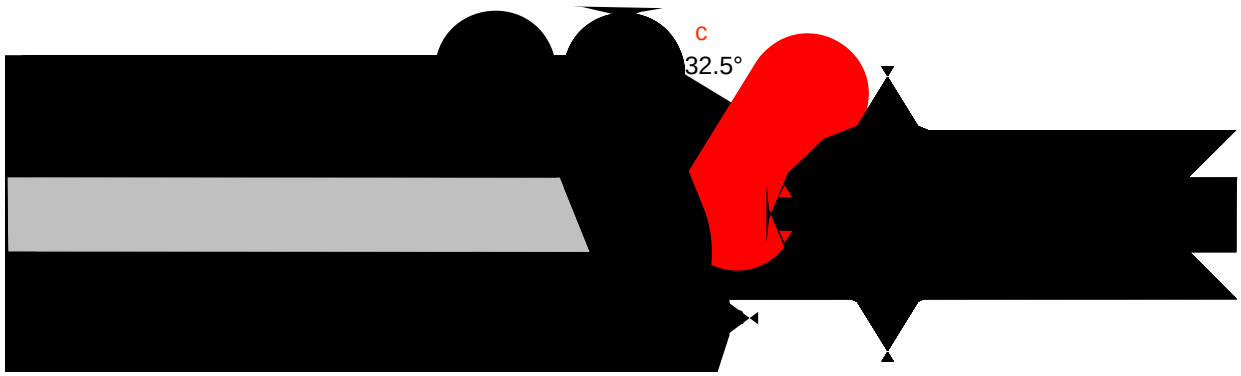

Figure 3. Steel plate arrangement for V-groove wet welds.

A hyperbaric chamber and a gravity welder were used to perform the wet welds during this project. This equipment is shown in Figure 4.

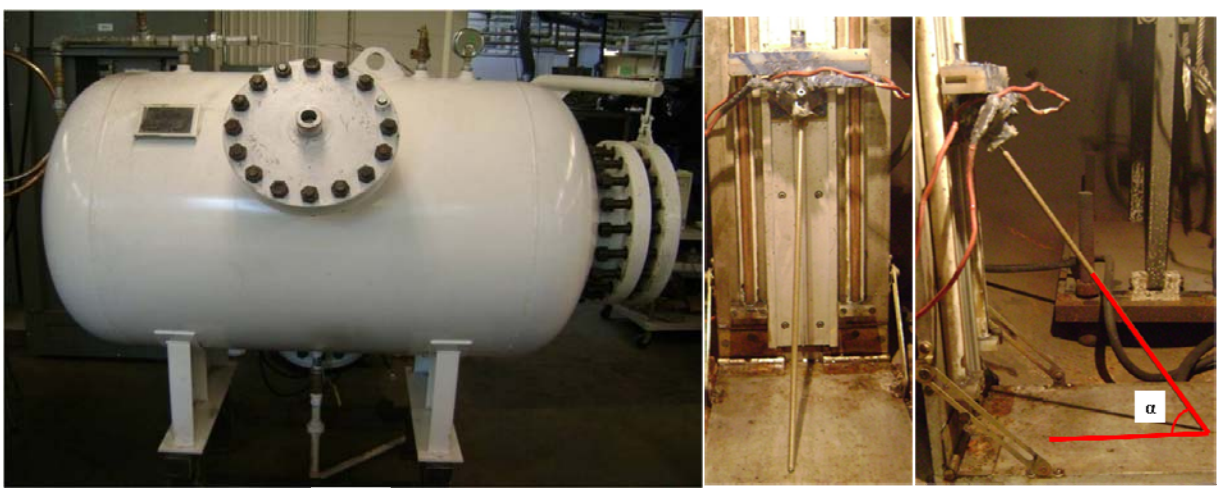

(a) (b)

Figure 4. Hyperbaric chamber (a) used to perform the wet welds with the gravity welder (b) placed inside the chamber. The angle α between the electrode and base plate is also defined.

Several tests were made to determinate the best welding parameters for each one of the electrodes. Using the "wet 1" electrode extruded at CSM, the polarity and the angle between base plate and electrode (α) were the same as those used in the previous phases of this project. Several tests using direct current electrode positive (DCEP) and an angle of 55°, were made to identify the best welding currents that could be used with this electrode, as shown in Table 2. The best parameters selected are shown in Table 3.

Table 2. Experimental matrix of "wet 1" extruded at CSM, used during initial tests.

Test	Velocity (mm/s)	Current average (A)	Voltage average (V)
Tests at 100 ft.			
1	2.9	170	25
2	2.6	172	26
3	2.4	162	28
4	2.8	154	22
Tests at 200 ft.			
1	3.6	194	22
2	2.7	182	29
3	3.4	187	21
4	2.8	179	24
Tests at 328 ft.			
1	2.6	190	27
2	2.6	190	31
3	3.7	187	21
4	3.3	208	22

Table 3. Selected parameters for "wet 1" electrodes extruded at CSM.

Test	Velocity (mm/s)	Current average (A)	Voltage average (V)
Tests at 100 ft.			
3	2.4	162	28
Tests at 200 ft.			
2	2.7	182	29
Tests at 328 ft.			
2	2.6	190	31

Using the same electrode, tests were also made using direct current electrode negative (DCEN) with an angle of 55° at 328 ft., as shown in Table 4. These tests were made to improve weld penetration, in an attempt to keep the same weld quality as observed in the DCEP welds.

Table 4. Experimental matrix of "wet 1" extruded at CSM, using DCEN at 328 ft.

DCEN Tests at 328 ft.			
Test	Velocity mm/s	Average Current A	Average Voltage V
1	2.5	196	19
2	2.7	206	20
3	2.9	213	23
4	2.9	220	23
5	2.9	229	23
6	2.8	236	24
7	2.9	243	24
8	3.0	251	25
9	3.0	252	26
10	3.1	255	27
11	3.1	256	28
14	3.2	264	26
15	3.1	255	28
12	2.9	249	29
13	3.1	263	26

As the fabricating process used by Devasco, International to produce the electrodes was different from that followed by CSM, it was necessary to conduct some tests with their electrodes before making welds for analysis. Tests were made using DCEP; the angle between the electrode and base plate, and the welding current were changed. Table 5 shows tests made at 1 ft. water depth and Table 6 shows tests made at 200ft. water pressure.

Table 5. Experimental matrix of "wet 1" extruded at Devasco, International, at 1 ft.

Tests Made Using Electrode Extruded at Devasco, at 1 ft.					
Test	Electrode Angle	Average Current (A)	Average Voltage (V)	Velocity (mm/s)	Obs.
1	45	184.4	21.7	3.4	Weld Stopped; Short Circuited
2	45	189.5	22.2	3.4	
3	45	195.1	21.3	3.4	
4	45	205.5	21.1	3.5	
5	50	180*	-	-	Weld Stopped; Short Circuited
6	50	200*	20.6	3.2	
7	50	220*	20.2	3.4	

* - Nominal set current, not from actual reading.

Table 6. Experimental matrix of “wet 1” extruded at Devasco, International, at 200 ft.

Tests Made Using Electrode Extruded at Devasco, at 200 ft.					
Test	Electrode Angle	Average Current (A)	Average Voltage (V)	Velocity (mm/s)	Obs.
1	45	240.8	21.0	4.8	
2	45	252.6	20.2	5.1	
3	45	256.8	19.7	5.2	
4	45	261.0	20.8	5.3	
5	45	271.0	22.1	5.2	
6	45	280.4	21.0	5.3	
7	45	272.7	25.5	5.0	
8	45	295.2	20.6	5.6	
9	45	279.1	26.0	5.1	
10	47	273.6	20.7	5.0	
11	47	269.9	25.9	4.9	
12	47	272.7	25.6	4.9	
13	47	290.2	21.9	5.2	
14	47	294.8	22.6	-	
15	47	294.1	22.0	5.2	
16	47	300.8	21.4	5.2	
17	50	184*	-	-	Weld Stopped; Short Circuited
18	50	230*	-	-	Weld Stopped; Short Circuited
19	50	273.5	22.4	4.5	
20	50	278.0	24.4	4.7	
21	50	281.6	23.8	4.7	
22	50	291.4	22.0	4.8	
23	55	237*	-	-	Weld Stopped; Short Circuited
24	55	256.6	19.5	4.2	
25	55	259.5	21.7	4.3	
26	55	262.3	23.1	4.4	
27	55	281.8	21.0	4.3	
28	55	288.8	20.8	4.3	
29	55	288.0	22.5	4.4	
30	55	295.7	22.3	4.4	
31	55	300.8	21.4	4.6	

* - Nominal set current, not from actual reading.

For weld bead morphology, hardness measurements and microstructural analysis, three transverse cross-sections were removed from each weld bead, one at the beginning (40 mm from weld start), one at the middle and one at the end (20 mm from the weld crater). The samples were prepared following standard metallographic procedures and etched with a 2% Nital solution, and photographed. Gravimetric method was used to quantify weld metal porosity. In this technique, porosity data is obtained by comparing the densities of the base metal and the weld metal. For each depth, two measurements were made, using two 20-mm long samples removed from the weld bead. A detailed procedure for this method is presented in the Appendix A.

Quantitative microstructural analysis was made on each weld bead at three spots, as shown in Figure 5. Several microhardness indentations were made along the two lines shown in Figure 6, and on three samples per depth from the same weld bead. Figure 7 shows how samples were prepared for chemical analysis using optical emission spectrometry (OES).

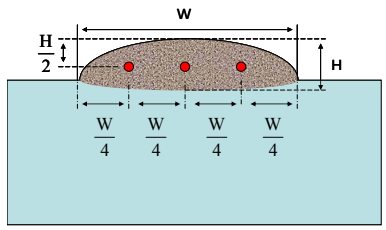

Figure 5. Schematic drawing showing the spots analyzed for microstructure.

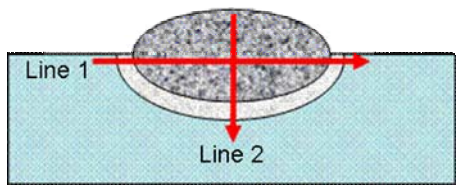

Figure 6. Schematic showing the location of the indentations.

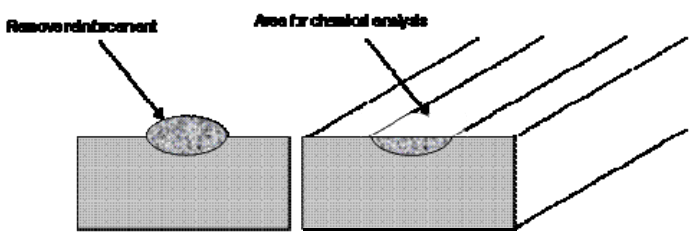

Figure 7. Schematic drawing showing the steps of sample preparation for chemical analysis.

4. RESULTS

The experimental results will be presented and discussed according to the following order: porosity in wet welds; bead-on-plate welding experiments: microstructures, chemical composition, and hardness; and V-groove welds.

4.1. Wet welds made using "wet 1" electrodes extruded at CSM

4.1.1. Porosity of wet welds

In the current project the strategy was to combine the results from all the previous projects into only one electrode formulation. Figure 8 shows bead-on-plate welds made at 100 ft. (30.5 m.), 200 ft. (61.0 m.) and 328 ft. (100 m.). As can be seen, the welds presented no undercutting, and well distributed ripples. Welds made at 100 ft. and 200 ft. presented no

superficial pores. The weld made at 328 ft. presented some superficial pores, but it has good quality for this water depth.

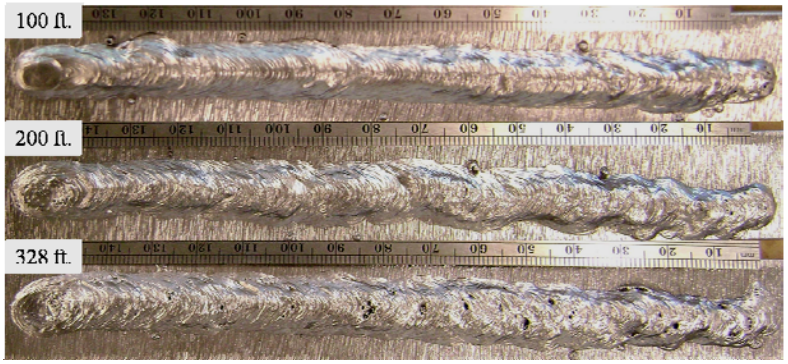

Figure 8. Wet weld made using "wet 1" electrodes extruded at CSM.

Table 7 shows the welding parameters used for these welds and the porosity quantification results. The porosity averages were 0.52 %, 1.46 % and 4.61 % in the welds made at 100 ft. (30.5 m), 200 ft. (61 m) and 328 ft. (100 m), respectively. As expected, porosity increased with increasing depth. Figure 9 shows macro-photographs taken from the middle section of the welds. The middle section tends to show an average porosity and dimensions when compared with the beginning and end of the weld. Note the low level of porosity even for the 328 ft. (100 m) weld. In contrast, Suga and Hasui (1986) reported around eight percent porosity for 50 m water depth and Rowe and Liu (2002) reported two percent in welds made at 60 m water depth. Substantial progress in porosity has indeed been accomplished.

In the last phase of this project (2007), it was reported an average of 0.33 pct. porosity in the welds made at 50 m (164 ft.) with the electrode F65; the amount of porosity was determined using metallographic techniques. In this method, the porosity is quantified by determining the ratio between the total weld area and the area of the pores in each cross section.

Porosity values should further decrease when using electrodes produced by a commercial electrode manufacturer because of the smaller variability in terms of flux coating thickness and core rod eccentricity. Greater extrusion pressure and more consistent extrusion will generally produce better quality electrodes. Porosity values also should decrease using manual welding instead of gravity welding, because gravity welding is not able to compensate for any electrode weldability differences or variations in plate/joint conditions.

Table 7. Porosity quantification. “wet 1” electrodes extruded at CSM.
NSC – Number of Short Circuits during 10th and 15th second of the weld.
Short circuit event was considered as each time when voltage reading was below 5 volts.

Depth (ft.)	Velocity (mm/s)	Voltage (Volts)		Current (Amperes)		NSC	Porosity %	
		Mean	Standard deviation	Mean	Standard deviation		1	2
100	2.5	27.7	6.0	160.3	56.0	17	0.78	0.27
200	2.8	29.3	8.3	178.6	63.7	21	1.42	1.5
328	2.8	28.8	9.8	189.1	66.6	8	4.54	4.69

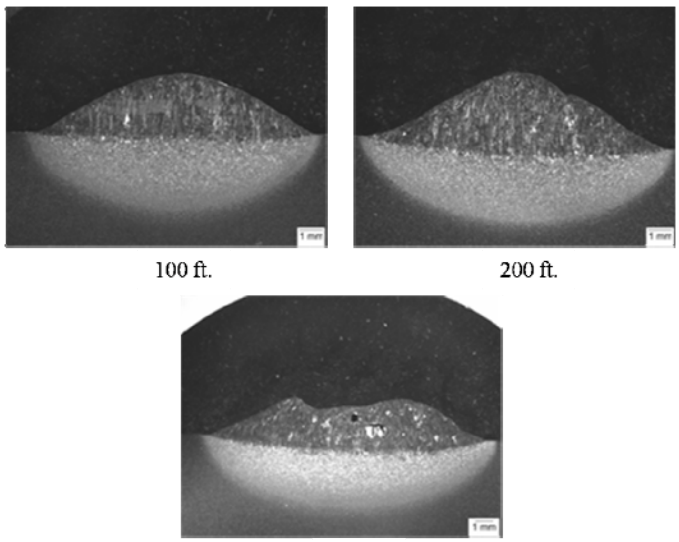

Figure 9. Weld bead macro-photograph extracted from the middle section of the welds.

4.1.2. Bead-on-Plate Wet Welds

This section presents BOP wet welds deposited with the experimental electrode at 100 ft. (30.5 m), 200 ft. (61 m) and 328 ft. (100 m) water depth. Arc stability, metal transfer mode, macro- and micro-structures, hardness and chemical composition are reported.

Figures 10, 11 and 12 show welds made at 100 ft., 200 ft. and 328 ft., respectively. As can be seen, all welds presented good morphology and wetting and exhibited no undercut. Welds made at 100 ft. and 200 ft. presented no superficial pores, and welds made at 328 ft. presented some superficial pores, but regarding the water depth, these welds can be considered as having very good welds. All welds presented easy slag detachability, with self-detaching slags in some parts of the beads. It is well known that slag plays an important role in the degasification of the weld metal, allowing gas evolution from the molten weld metal.

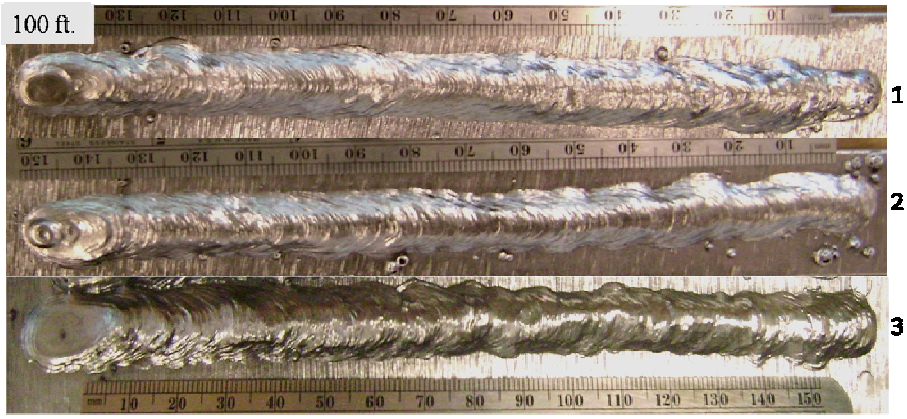

Figure 10. Wet welds made at 100 ft. using “wet 1” electrodes extruded at CSM.

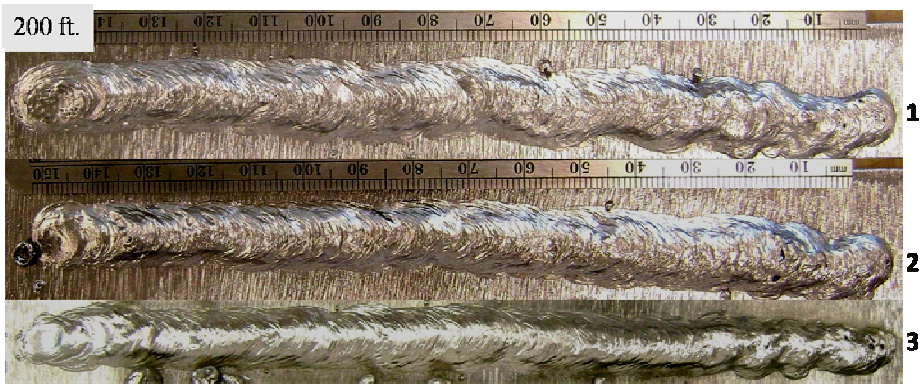

Figure 11. Wet welds made at 200 ft. using “wet 1” electrodes extruded at CSM.

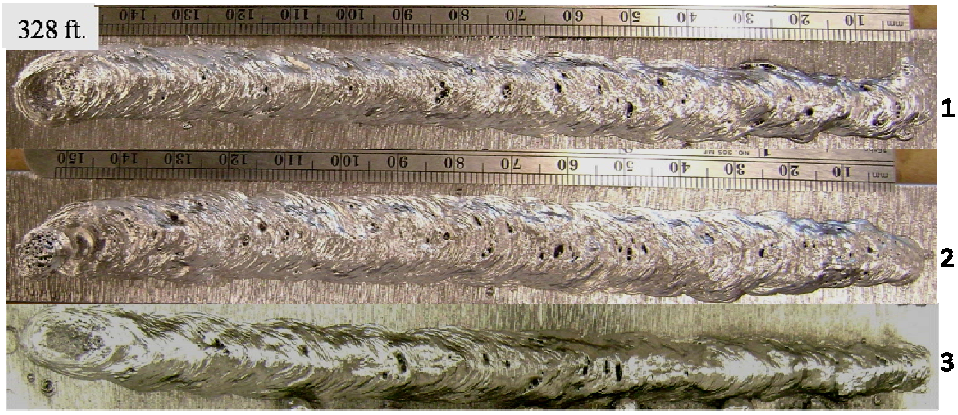

Figure 12. Wet welds made at 328 ft. using “wet 1” electrodes extruded at CSM.

Figures 13, 14 and 15 show the voltage signals of the welds made at 100 ft., 200 ft. and 328 ft., respectively, taken between 10th to 15th second during welding. Table 8 summarizes these signals. Voltage fluctuations are good indicators of metal transfer modes in welding. Large

voltage fluctuations from the mean process voltage greater than 20 volts are generally associated with short circuiting transfer. During short circuiting, welding voltage also tends to approach zero. Small voltage fluctuations around one volt are typical of spray transfer. Finally, intermediate fluctuations at the order of 10 volts indicate the occurrence of globular transfer. Based on these criteria, the predominant metal transfer mode at all water depths is globular. Very little short circuiting transfer occurred, which is reflected in reduced weld metal porosity. The large values observed in the voltage signals could also indicate that the steel rod was burning back, resulting in longer arcs.

Based on the voltage signals, it can be concluded that the arc was more stable at 100 ft. than at 200 ft. and 328 ft. This observation has been described by many researchers. More recently, Pessoa (2003) reported that when increasing the water depth and the ambient pressure, the arc became more constricted making it more unstable. Another way to infer arc stability can be through slag detachability. Unstable arc usually produces weld beads that exhibit irregular surface morphology with slag coverage that is difficult to remove. As discussed earlier in this report, all welds presented easy slag detachability, and often self-detaching, indicating reasonable to good arc stability.

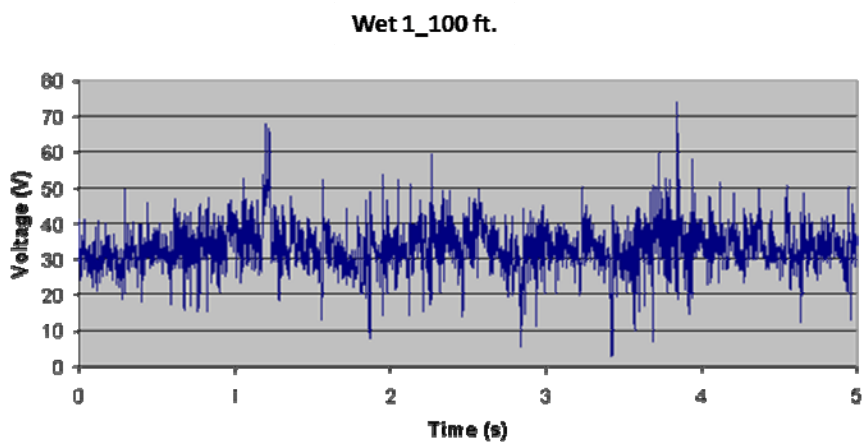

Figure 13. Arc voltage signal from the BOP wet weld made at 100 ft.

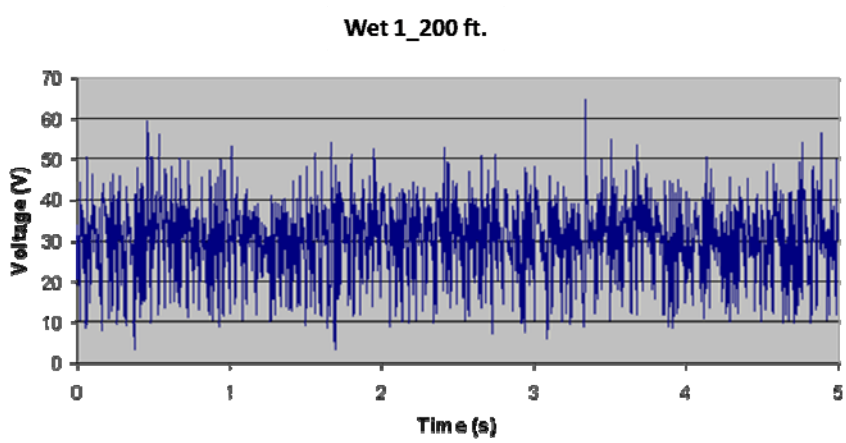

Figure 14. Arc voltage signal from the BOP wet weld made at 200 ft.

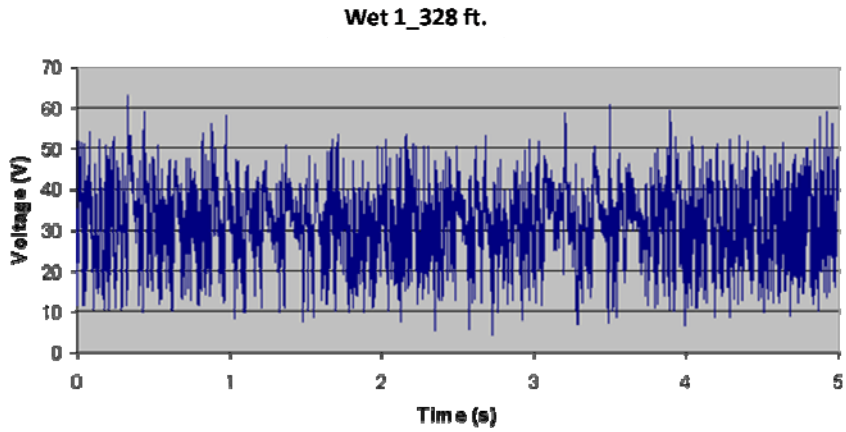

Figure 15. Arc voltage signal from the BOP wet weld made at 328 ft.

Table 8. Summary of the weld parameters.
NSC => Each time when voltage reading was below **5** volts.

Depth (ft.)	Velocity (mm/s)	Voltage (Volts)		Current (Amperes)		NSC
		Average	Standard deviation	Average	Standard deviation	
100	2.4	33.4	6.2	156.8	55.7	1
	2.5	28.5	6.4	159.4	56.7	20
	2.4	23.3	6.7	162.1	55.5	39
Average	2.4	28.4	6.4	159.4	56.0	20
200	2.8	28.9	7.2	179.6	61.6	7
	2.8	30.3	8.1	179.9	62.5	2
	2.9	29.3	7.4	178.0	61.2	4
Average	2.8	29.5	7.6	179.2	61.7	4
328	2.9	30.7	9.6	188.3	65.7	2
	2.8	31.8	9.6	187.9	66.1	1
	2.7	28.7	9.5	188.7	66.7	18
Average	2.8	30.4	9.5	188.3	66.1	7

Macro- and micro-photographs were made for metallographic analyses on the wet weld beads. Three cross-sections were made for each bead, at the beginning, middle and end of the weld. Figure 9 shows the macro-photographs taken from the middle section of the weld and Table 9 shows the measured weld bead morphology values. As can be seen, with increasing water depth (pressure), weld width, penetration, and heat affected zone (HAZ) width all increased. In contrast, reinforcement and wetting angle decreased. Surface porosity and top bead irregularities were observed to increase with increasing depth. All beads exhibited limited penetration, which can be improved by a welder/diver or switching to direct current electrode

negative (DCEN) provided that it does not increase weld porosity. As reported by Bracarense et al. (2003) and Liu and Perez (2004), rutile grade electrode produced higher porosity using DCEN than DCEP.

Table 9. Weld bead morphology values.

Depth ft.	Width mm	Reinforcement mm	Penetration mm	Angle	HAZ Sides mm	HAZ Bottom mm	Deffects
100	11.7	3.0	0.5	34.8	0.6	2.8	Few Pores
200	13.1	2.8	0.7	28.4	0.5	3.0	Few Pores and Bead Irregularities
328	14.9	2.7	0.7	27.5	0.5	3.5	More Pores and Bead Irregularities

The microstructure was photographed from locations indicated in Figure 5 at 200, 500 and 1000x magnification. Figure 16 shows three microphotographs from the middle spot on the welds using 200x magnification, and Figure 17 shows the microstructure quantification results. As can be seen, the dominant microstructures observed were ferrite with second phase, aligned and non-aligned [FS(A) and FS(NA)], primary ferrite [PF(G) and PF(I)] and martensite (M). Only small pockets of acicular ferrite (AF) were observed. Inclusions and microcracks were also found. Figure 18 shows the microstructure of the welds in the vicinity of the fusion line where evidence of epitaxial growth can be seen.

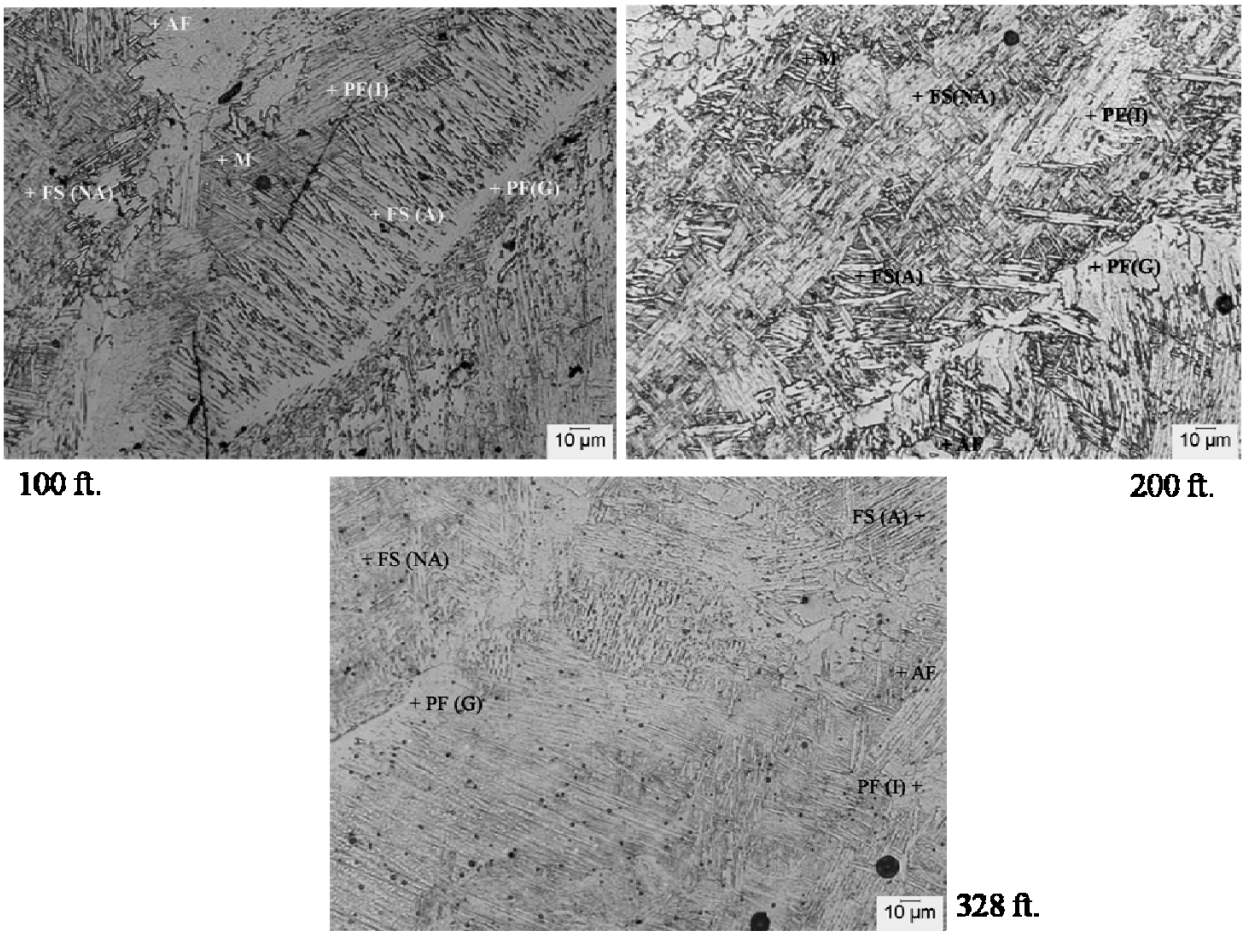

Figure 16. Weld bead microstructure.

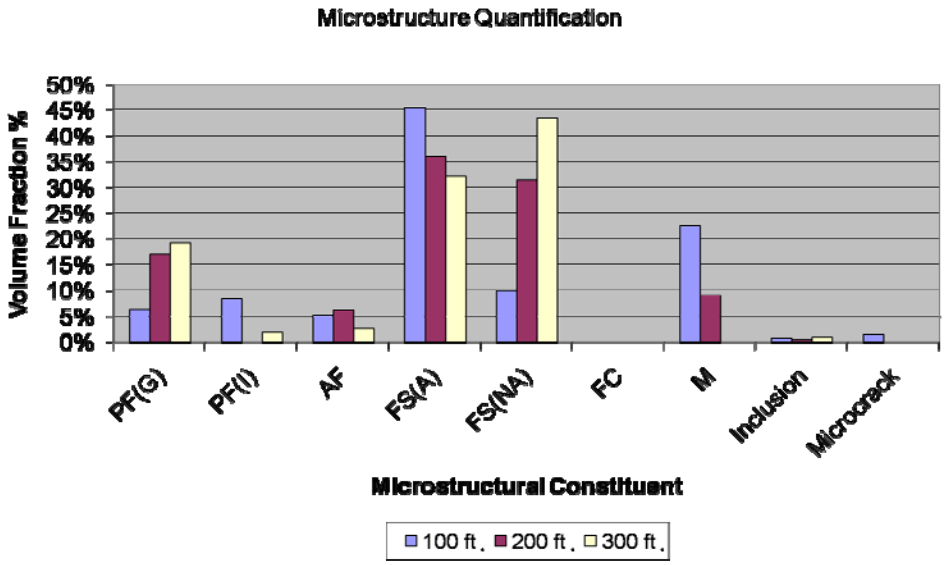

Figure 17. Weld bead microstructure quantification.

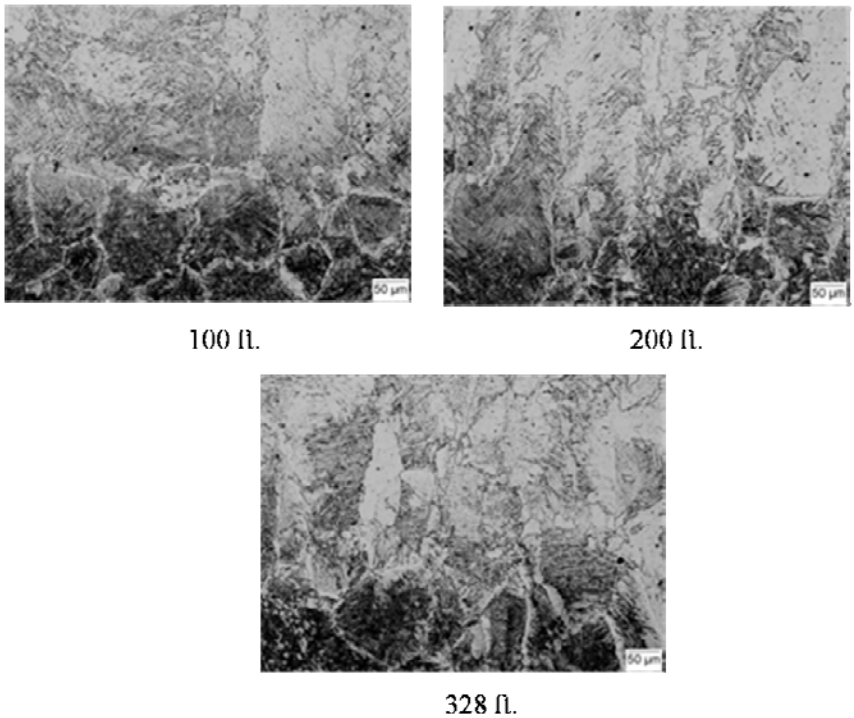

Figure 18. Weld bead microphotographs from fusion line illustrating epitaxial growth.

Microhardness indentations were made according to the locations shown in Figure 6, and Figures 19 and 20 show the results on line 1 and line 2, respectively. All hardness readings including heat affected zone and weld metal were below 300HV, acceptable for wet weld qualification.

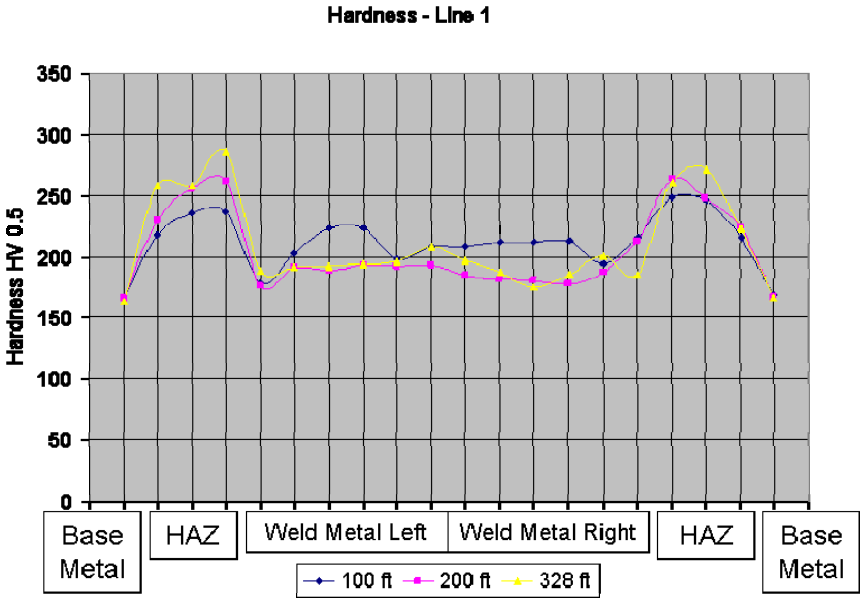

Figure 19. Micro hardness measured on line 1 (horizontal).
The horizontal line of the bead was divided into 20 intervals to make the indentations.

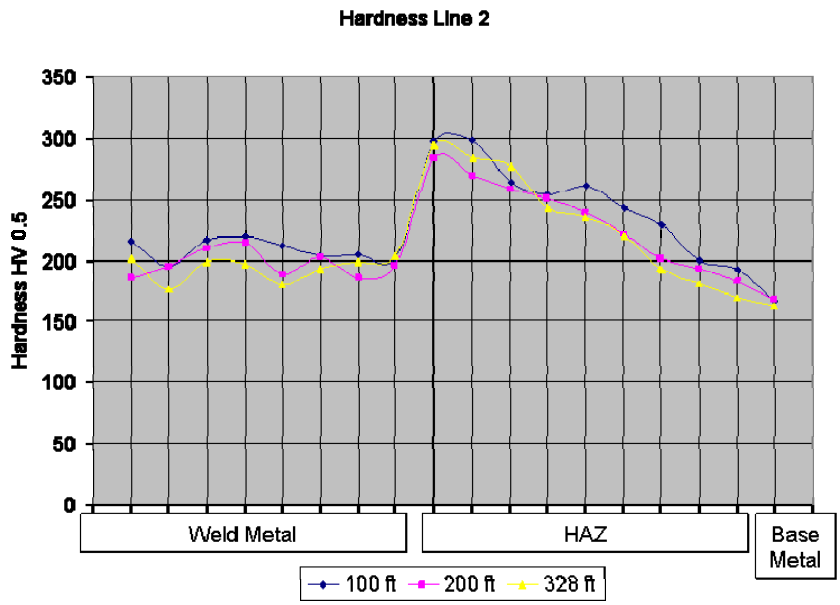

Figure 20. Micro hardness measured on line 2 (vertical).
The vertical line of the bead was divided into 18 intervals to make the indentations.

Table 10 shows chemical analyses made on the weld metals. Two analyses were made for each depth and the results were presented as average values. Figure 21 shows weld metal chemical composition variation with water depth. Figures 22 and 23 compared current compositions with previous weld chemistry as reported by Rowe (1999) and Perez (2003). The current electrodes recovered higher amounts of manganese and silicon confirming that the flux system provided better protection against oxidation losses with increasing water depth.

Table 10. Chemical analyses made on weld metal.

Element	Depth ft.		
	100	200	328
CARBON	0.08	0.08	0.08
SULFUR	0.01	0.01	0.02
PHOSPHORUS	0.02	0.03	0.02
SILICON	0.31	0.09	0.12
CHROMIUM	0.04	0.03	0.04
NICKEL	1.53	1.54	1.40
MANGANESE	0.59	0.25	0.31
COPPER	0.10	0.08	0.10
MOLYBDENUM	0.01	0.01	0.01
COLUMBIUM	0.01	0.02	0.02
TITANIUM	0.02	0.02	0.02
ALUMINUM	0.01	0.01	0.02
VANADIUM	0.01	0.01	0.02
COBALT	<0.01	<0.01	<0.01
TUNGSTEN	0.01	0.02	0.02
IRON	Base	Base	Base

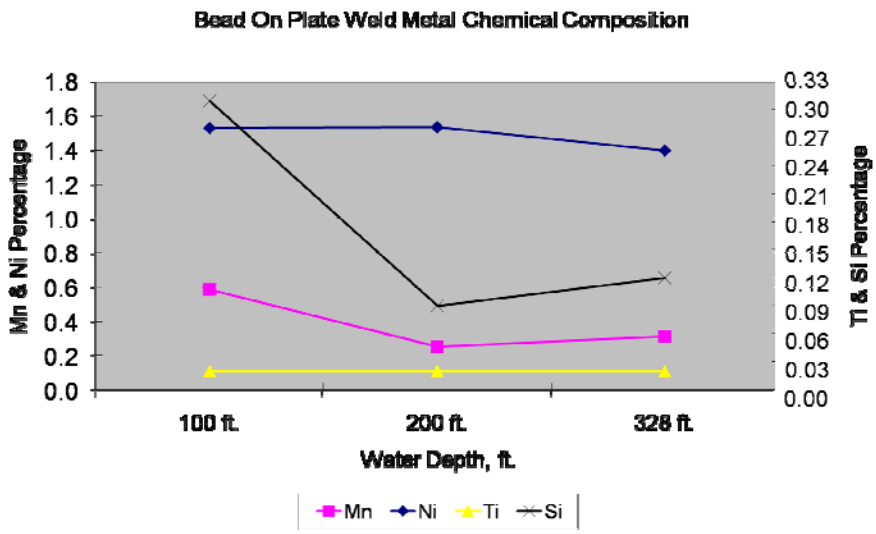

Figure 21. Weld metal chemical composition variation with water depth.

As can be seen and expectedly, the loss of alloying elements increased with increasing water depth. However, the nickel content was still below the targeted value of around 2 to 2.2 wt. pct. and the titanium content was short of the preferred 300 to 400 ppm level. The manganese concentration was also slightly lower than the designed value by about 10%. The compositional difference may have contributed to the lower than desired acicular ferrite content in the weld metals. The electrode flux composition will be reiterated to fine tune the flux and reach the design values.

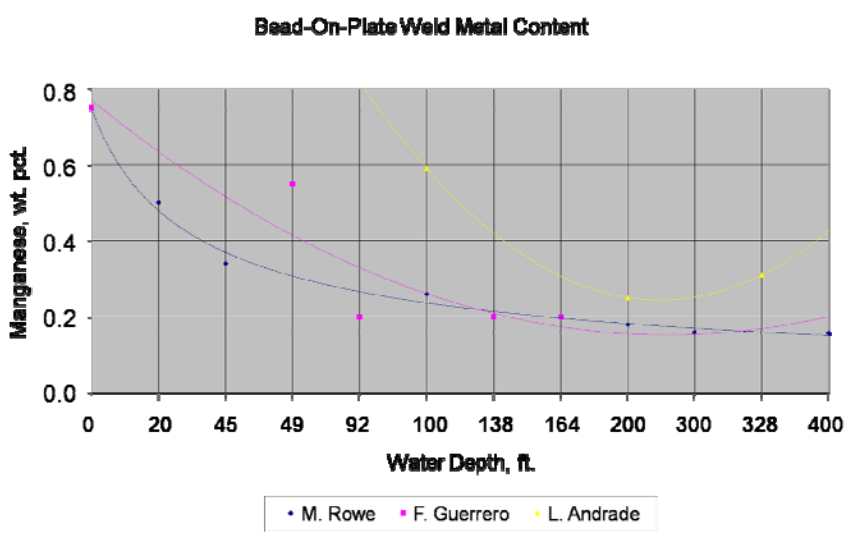

Figure 22. Weld metal manganese concentration compared with prior works (M. Rowe, 1999; F. Guerrero, 2003)

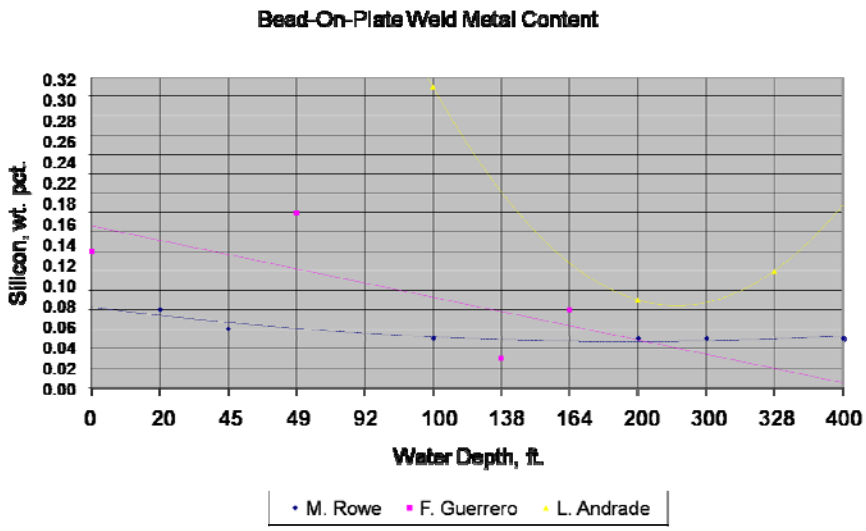

Figure 23. Weld metal silicon concentration compared with prior works (M. Rowe, 1999; F. Guerrero, 2003)

4.1.3. V-Groove Wet Welds

Multipass V-groove wet welds were deposited with the experimental electrodes to make specimens for mechanical testing. During multipass wet welding the following problems were observed: arc instabilities, lower voltage values, short circuiting transfer (particularly in the beginning side of each weld pass), and surface pores. As observed in previous phases of this project as well as reported by other researchers, the wet weld passes exhibited more porosity in the beginning side than in the middle section and end side of the welds. Despite the several attempts made, some weld passes still presented this problem.

Figure 24 shows the different bead quality made at 328 ft. using selected electrodes using the same parameters. As can be seen, some welds presented poor quality along all bead length (A), while others presented poor quality in the beginning of the bead, but good quality in the end (B). Other welds presented good quality along all bead length (C). This problem happened independent of the water depth. One possible cause of the arc instabilities could be the flux thickness variations in the electrodes. Therefore, it was decided that V-groove wet welds would be made using only electrodes extruded at Devasco, International which have better quality than electrodes extruded at CSM.

Figure 24. Different bead quality obtained at 328 ft. using selected CSM electrodes after extrusion. A – Poor quality along all bead length; B – Poor quality in the beginning of the bead, but good quality at the end of the bead; C – Good quality along all bead length. Scale in millimeters.

V-groove welds were made at 100ft., 200ft., and 328ft. After welding, the V-grooved welds were radiographed. The radiographic films of the weld made at each water depth are shown in Figure 26. High porosity resulted, not totally unexpected, particularly in view of the earlier bead-on-plate results. The only difference from previous multipass welds was in the V-groove dimensions. When the included angle and root gap opening are small, as shown in Figure 25, electrode accessibility is poor, erratic arc will result and molten metal flow will become more restricted, trapping the gases in the solidified metal. To mitigate the porosity question and correct the V-groove design, a different V-groove was selected. The proposed dimensions of this new V-groove were showed in Figure 3.

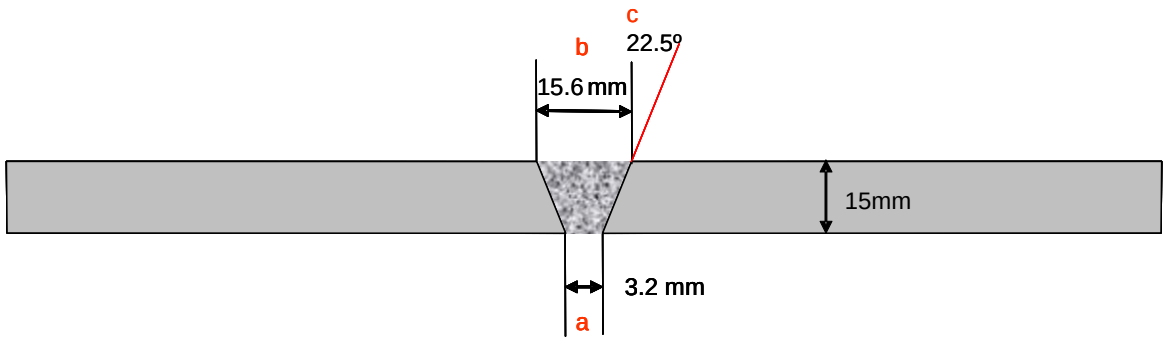

Figure 25. First steel plate arrangement used for V-groove wet welds.

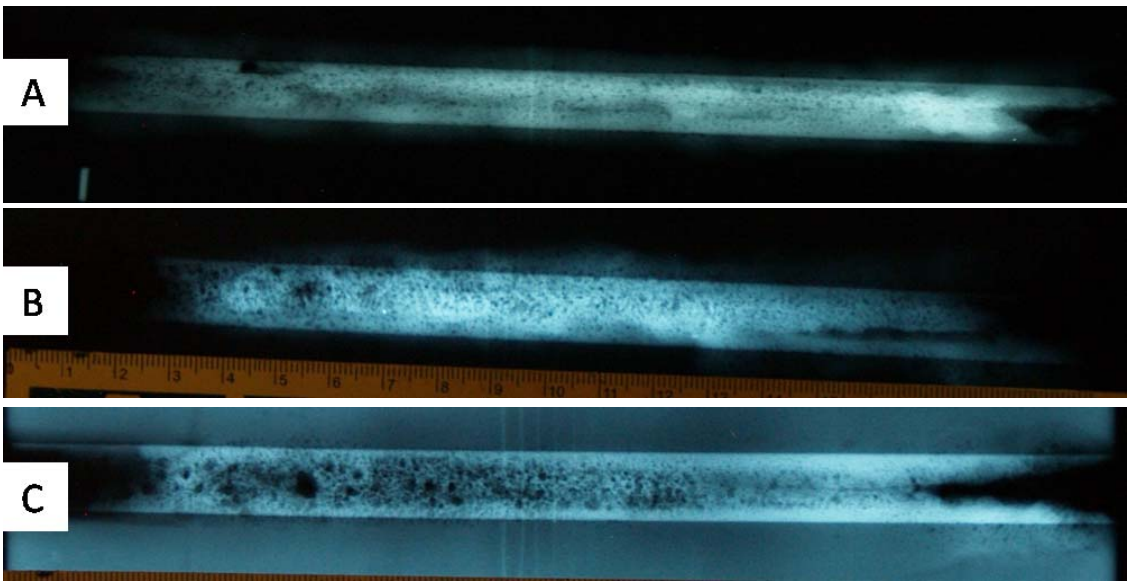

Figure 26. V-groove radiographic films. A – 100ft.; B – 200 ft.; C – 328ft.
Left side is the beginning of the weld.

Figures 27, 28 and 29 show typical voltage signals acquired during V-groove wet welding at 100 ft., 200 ft. and 328 ft., respectively. As can be seen, the electrodes produced large droplets (indicated by the large variations in voltage) that were filled with gas to result in weld metal with high porosity. Contrary to what was observed in the BOP wet welds, all V-groove welds showed short circuiting as the predominating transfer mode. In the weld made at 328 ft (Figure 29), as the weld progressed, the average voltage increased slightly, but changing from short circuiting to globular metal transfer mode. This behavior may be the result of electrode rod heating that released the droplet prior to short circuiting. This same trend was reported in the last phase of this project (2007).

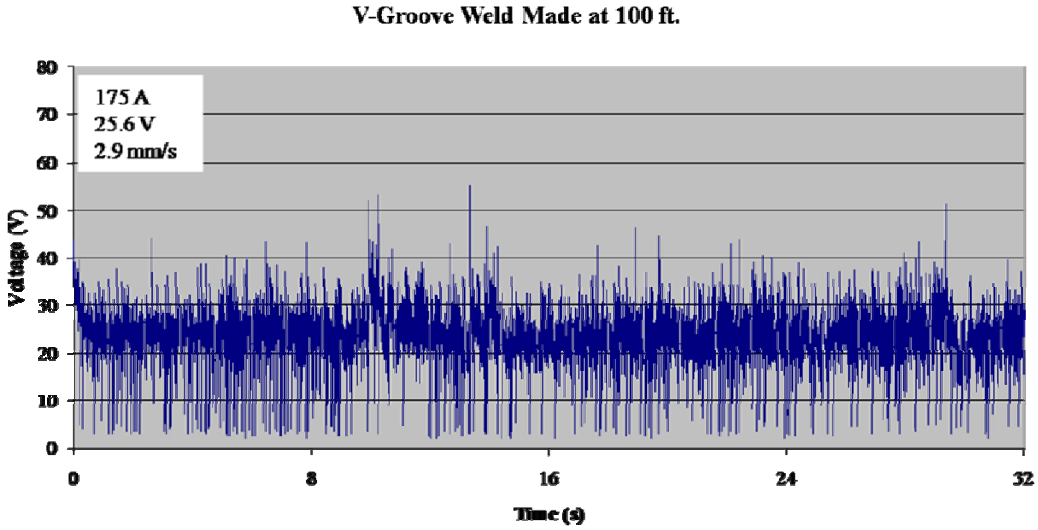

Figure 27. Typical voltage signal acquired during V-groove wet welding at 100 ft.

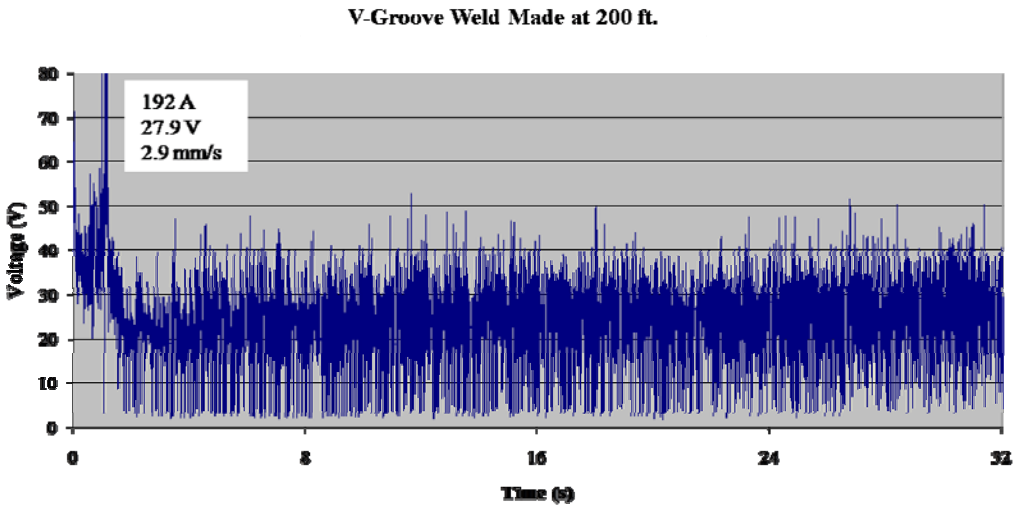

Figure 28. Typical voltage signal acquired during v-groove wet welding at 200 ft.

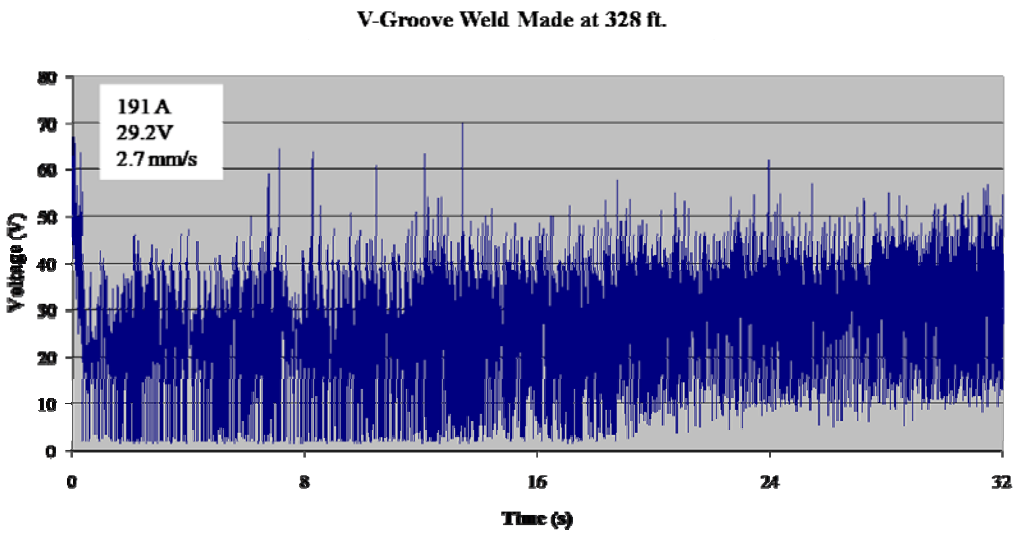

Figure 29. Typical voltage signal acquired during V-groove wet welding at 328 ft.

Considering the poor quality of the V-groove wet welds produced with CSM "wet 1" electrodes confirmed by the radiographs shown in Figure 26, it was considered unnecessary to produced specimens for mechanical testing.

4.2. Wet welds made using “wet 1” electrodes extruded at Devasco, International

As presented in previous reports and discussions, the formulations developed at the Colorado School of Mines will need to be transitioned to a consumable industry for fine tuning and scale up for industrial production. Devasco, International has been identified as the company that will make the adaptation and the product industrially feasible. A multi-stage systematic approach is often required to work through the differences between the two manufacturing

facilities in terms of equipment characteristics (flux batch size, ram pressure, etc.), ambient characteristics (mainly relative humidity), and raw material characteristics (mineral substitution, mineral supplier, particle size distributions, slipping aid, and binder type and amount). After extrusion, tests will also need to be conducted to determine the welding parameters for the new electrodes.

Several tests were conducted at Devasco, International to identify the parameters for good quality welds following the procedures used for the CSM extruded electrodes shown in Tables 5 and 6. The welds produced at 1 ft. water depth presented excellent surface morphology, with no external pores as expected and no undercutting. However, the good surface quality was anticipated considering the shallow water depth. Figure 30 shows a typical weld photograph of the welds made at 1 ft., and Figure 31 shows the typical voltage signals during welding. As can be seen, during the entire welding, short circuiting was the predominant metal transfer mode. All welds made using this electrode at this water depth presented similar performance.

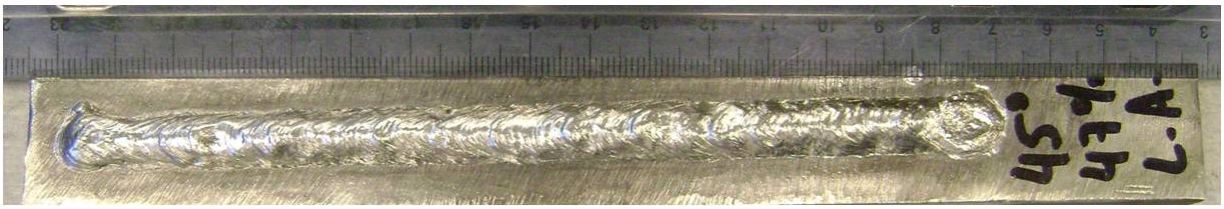

Figure 30. Typical weld produced using "wet1" electrodes extruded at Devasco, International, at 1 ft. water depth.

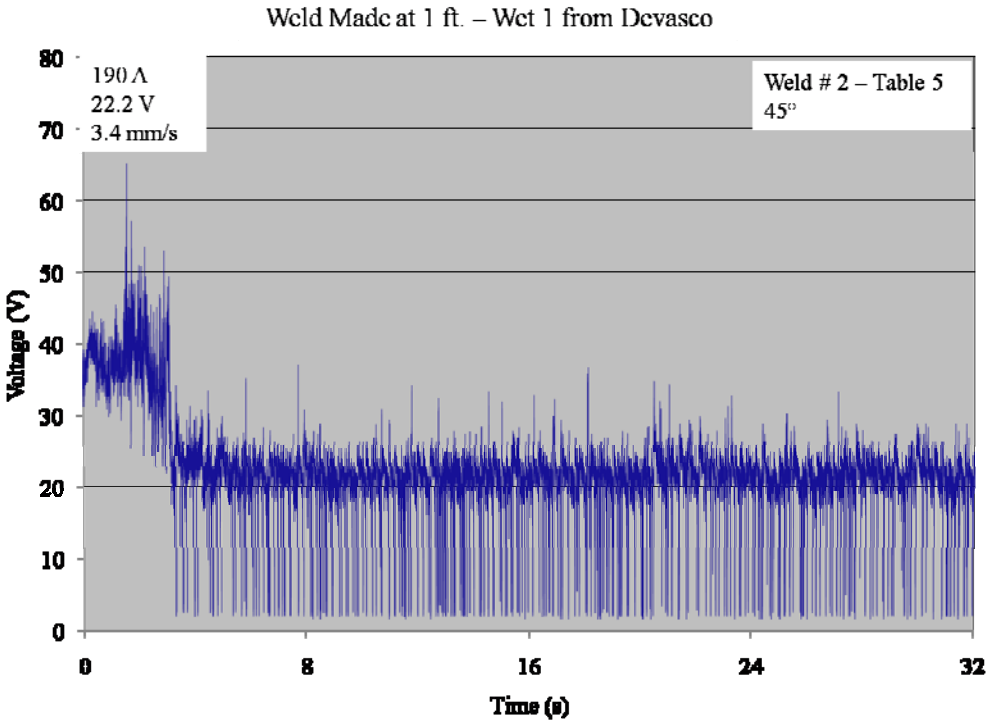

Figure 31. Typical voltage signals from welds made at 1 ft. water depth, using "wet 1" electrodes extruded at Devasco, International.

The welds produced at 200 ft. did not produce the good quality found in the welds produced using the electrodes extruded at CSM. Even the best welds showed many defects such as external pores, irregular beads and high porosity on the transverse cross sections shown in Figures 32, 33 and 34. These figures shows the best welds made using an angle between electrode and base plate of 45°, 47° and 50°, respectively, as well as the cross section from the best part of the bead.

Higher welding currents than those used with the electrodes extruded at CSM were necessary to produce welds with the electrodes extruded at Devasco, International. As shown previously in Table 3, the welding current used with electrodes from CSM was 182 amperes at 200 ft.; in comparison, the welding current used with electrodes from Devasco, International was around 275 amperes for the same water depth. Using the electrodes extruded at Devasco, International at low current values, the arc would not open or it would extinguish after arc opening. It is known (ASM Handbook, 1993) that high currents using DCEP produced more porosity in the weld metals than lower currents. The requirement of higher welding current could have contributed to the poor quality of the welds made using electrodes from Devasco, International.

A possible reason for the higher welding current necessary using the electrodes extruded at Devasco, International could be the different particle size distribution as well as the different drying and baking process used. At CSM, after electrodes extrusion, the electrodes were air dried at room temperature during 24 hours followed by oven baking at 300° F for 90 minutes. At Devasco, International, however, the electrodes were air dried at room temperature during 12 hours and then oven baked at 850° F for 120 minutes.

It is plausible that the higher temperature and time during the baking process resulted in a drier electrode flux covering than necessary. Another effect of the higher temperature and time during the baking process could be the oxidation of some elements of the electrode covering, and consequently loss of weldability properties of the electrode. These two effects would result in a higher welding current required for opening and maintaining the arc.

Another possible reason for the poor quality of the welds could be the lower arc voltage. Comparing the two electrodes, those manufactured by Devasco, International produced welds with voltage value around 25 volts and short circuit metal transfer mode, Figure 35, and the electrodes from CSM produced welds with voltage values around 29 volts and globular metal transfer mode. During his research, Perez (2007) concluded that short circuit metal transfer mode would produce higher porosity than globular mode. One possible reason for the lower arc voltage observed with the electrodes from Devasco, International could be the difference in the particle size distribution of the minerals used to extrude the electrodes. The minerals used by Devasco, International were finer than those used by CSM.

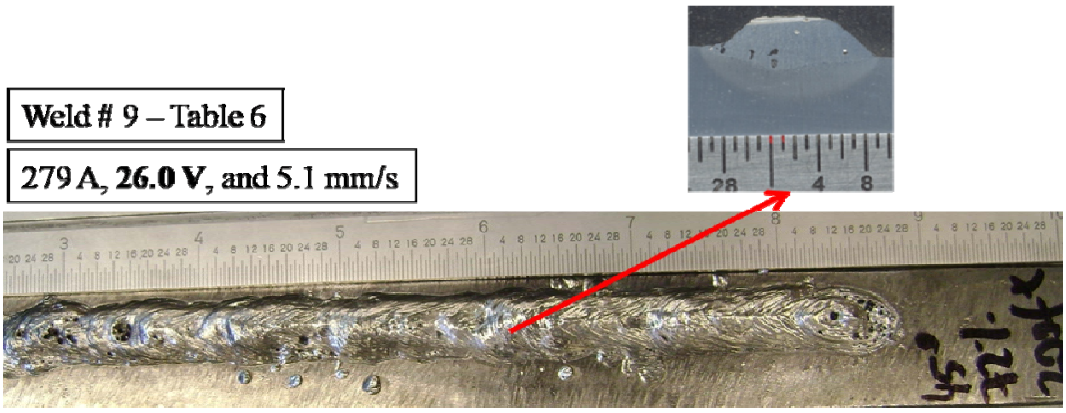

Figure 32. The best weld made at 200 ft. using an angle of 45°.

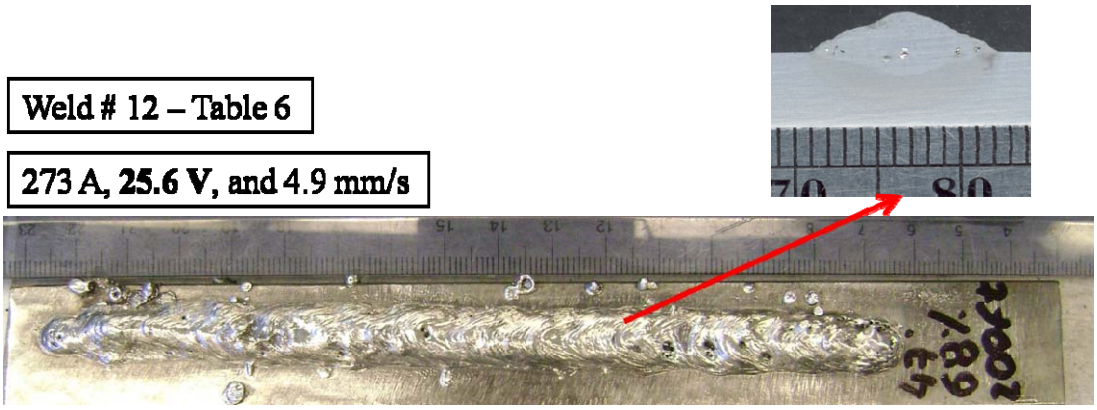

Figure 33. The best weld made at 200 ft. using an angle of 47°.

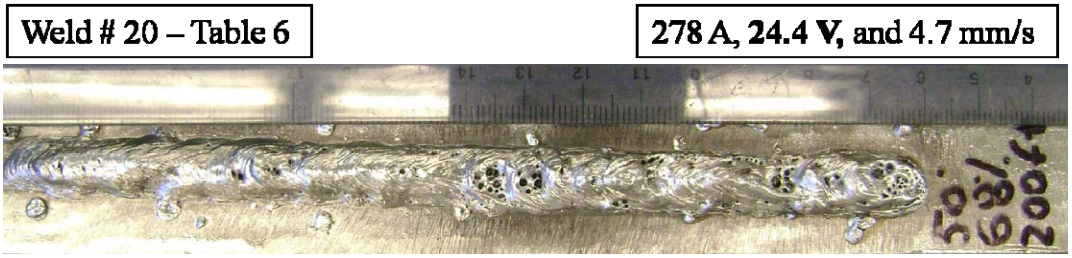

Figure 34. The best weld made at 200 ft. using an angle of 50°.

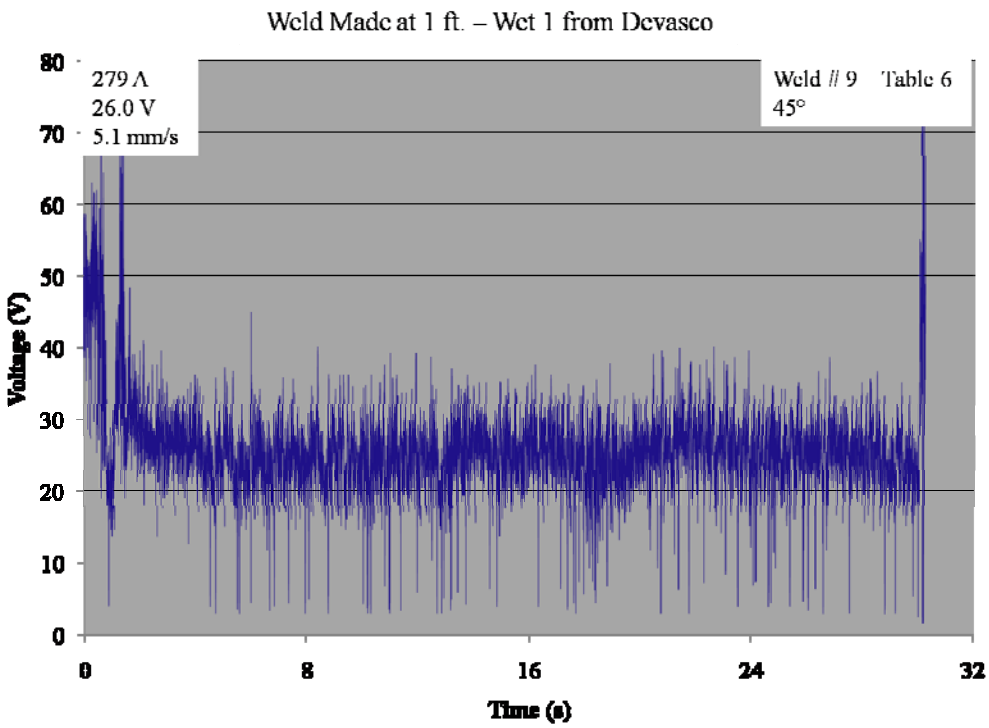

Figure 35. Typical voltage signals from welds made at 200 ft. water depth, using "wet 1" electrodes extruded at Devasco, International.

Based on the problems and poor quality of the BOP wet welds produced with "wet 1" electrodes from Devasco, International, V-groove wet welds for the purpose of mechanical testing were not deposited.

The electrodes "wet 2" (with higher alloy content to compensate for greater water depth) extruded by Devasco, International were manufactured using the same procedures than the electrodes "wet 1", and considering it, welds make using electrodes "wet 2" would present the same problem that welds made using electrodes "wet 1". For this reason, the electrodes "wet 2" were not tested.

Inability to match the exact compositions will unfortunately delay the final testing of these innovative electrodes to a future testing and qualification phase that is being organized at the time of this report. However, Devasco, International is committed to work with the Colorado School of Mines to continue the extrusion of new batches of electrodes for testing, albeit incrementally and at a slower pace in the future.

5. CONCLUSIONS AND RECOMMENDATIONS

Considering the experimental work conducted in this research program, the following conclusions and recommendations can be drawn.

5.1. Conclusions

Regarding the welds made using electrodes extruded at CSM with core rods that contain extra low nominal carbon content, 0.001 wt. pct.:

1. Porosity measured using the gravimetric method was very low, in the order of 1.5 % in wet welds made at 200 ft. (61 m).
2. Arc stability was good, as evidenced by low voltage fluctuations and easy slag detachability.
3. Globular metal transfer mode was the predominant metal transfer mode observed during welding.
4. Welds presented regular bead appearance and morphology, but with limited penetration.
5. Ferrite with second phase was the predominant microstructural component in the welds.
6. Recovery of alloying elements increased significantly, compared with prior works.

Regarding the welds made using electrodes extruded at Devasco, International:

7. Welds presented higher porosity and superficial pores.
8. Welding occurred with low arc stability, as evidenced by large voltage fluctuations.
9. Short circuiting was the predominant metal transfer mode during welding.
10. Welds exhibited irregular bead appearance, but deeper penetration than the ones made using the CSM extruded electrodes.

The inability to match the exact compositions will unfortunately delay the final testing of these innovative electrodes to a future testing and qualification phase that is being organized at the time of this report.

5.2. Further Considerations of the Results

The V-groove welding results using the Devasco electrodes were discussed with Devasco, International. According to the Devasco experts, the finer flux particle size was responsible for the low welding voltage and better arc stability. They also certified that the core rod carbon content as accurate, at the proximity of 0.001 wt.pct. The slightly lower nickel content can be easily corrected, without perturbing the weld pool chemistry. Adjustment of boron content may not be as simple since ferro-boron usually contains nitrogen. However, a substitution of ferro-born with nickel-boron can be made. With this latter alloy, both boron and titanium will be enriched, towards the target composition.

Subsequent chemical analyses conducted by an external laboratory proved that the carbon content was indeed low, with values between 0.0017 to 0.002 wt.pct. Devasco experts offered the view that carbon pick-up had occurred and likely from the waterproof coating. They suggested that CSM conduct a research to examine the effect of the varnish coating during welding since the tight control of carbon through electrode core rod can be easily offset by the carbon-rich waterproof coating.

5.3. Recommendations

1. Flux coatings with ingredients that had finer particle size distribution exhibited better extrudability. Flux coatings with ingredients with coarser particle size distribution exhibited higher welding voltage and less short circuiting transfer. The effect of particles size distribution should be investigated to improve the quality of the wet welds and reduce the porosity together with extra low carbon content core rods.
2. Determine the best temperature and time to bake the electrodes for the production of welds with lower porosity and better quality.
3. Develop joint industry research program (JIP) for the qualification of the electrodes developed in this phase of the work. The JIP program will: 1) produce electrodes that match the exact composition of the experimental welds using extra low carbon content rods and optimal flux particle size distributions; 2) qualify the electrodes for wet welding procedures for 200 ft. water depth.

6. ACKNOWLEDGMENTS

The researchers of this program acknowledge the continuous support provided by the Minerals Management Service, in particular Mr. Michael Else and Dr. Charles Smith (the earlier phases of this work). The assistance and discussion from Dr. Faustino Perez-Guerrero is invaluable for the progress of this research project. The researchers also wish to acknowledge the support of Devasco, International, in particular Mr. Joe Scott and Mr. Keith Moline.

7. REFERENCES

ASM Handbook. Welding, Brazing and Soldering. Vol. 6, ASM International, 1993.

BRACARENSE, A. Q. and PESSOA E. C. P. Wet Welding in Fresh Water. Second Report, Submitted to Colorado School of Mines, 2003.

FLOREEN, S., HAYDEN, H. W. and DEVINE, T. M. Cleavage Initiation in Fe-Ni Alloys. Metallurgical Transactions, Vol. 2, pp. 1403-1406, May, 1971.

LIU, S. and PÉREZ, F. Joint Research Program Between MMS and PEMEX/IMP Underwater Wet Welding for Offshore Structures and Pipelines in the Gulf of Mexico: Process Maturation and Technology Transfer. Final Report Submitted to the Minerals Management Service and Instituto Mexicano del Petroleo, August, 2004.

LIU, S. and PÉREZ, F. Joint Research Program Between MMS and PEMEX/IMP Underwater Wet Welding for Offshore Structures and Pipelines in the Gulf of Mexico: Enhanced Reliability and Integrity of Underwater Wet Welds. Final Report Submitted to the Minerals Management Service and Instituto Mexicano del Petroleo, November, 2007.

PÉREZ, F. Effect of Nickel Additions on Rutile Electrodes for Underwater Welding. Golden, Colorado, EUA, Colorado School of Mines. Thesis, 100f, 2003.

PÉREZ, F. The Mechanism of Porosity Formation in Underwater Steel Welds using SMAW Process. Golden, Colorado, EUA, Colorado School of Mines. Dissertation, 183f, 2007.

PESSOA, E. C. P. Estudo Comparativo do Desempenho de Eletrodos Comerciais E6013, E7018 e E7024 em Ambiente Molhado. Dissertação. Universidade Federal de Minas Gerais. Brasil, 2003.

PESSOA, E.C.P. Estudo da Variação da Porosidade ao Longo do Codão em Soldas Subaquáticas Molhadas. Programa de Pós-Graduação em Engenharia Mecânica, Belo Horizonte, Minas Gerais: Universidade Federal de Minas Gerais, Tese, 2007.

PESSOA, E. C. P., BRACARENSE, A. Q., LIU, S., and GUERRERO, F. P. Exothermic Additions in a Tubular Covered Electrode and Oxidizing Reactions Influence on Underwater Wet Welding, Proceedings of OMAE07. 26th International Conference on Offshore Mechanics and Arctic Engineering, June 10-15, 2007, San Diego, California USA.

POPE, A. M., TEIXEIRA, C. G., DOS SANTOS, V. R., PAES, M. P., and LIU, S. Use of Nickel to Improve the Mechanical Properties of High Oxygen Underwater Wet Welds. Proceedings: 14th Offshore Mechanics and Arctic Engineering Conference, June, 1995, Copenhagem, Denmark. American Society of Mechanical Engineers. Vol. III pp 529-535.

A. Sanchez-Osio, S. Liu, S. Ibarra, and D.L. Olson, "Designing Shielded Metal Arc Consumables for Underwater Wet Welding in Offshore Applications", ASME Journal of Offshore Mechanics and Arctic Engineering, 117 (8), pp. 212-220, 1995.

ROWE, M. D. Effect of Ferro-Alloy Additions and Increasing Depth on the Quality of Underwater Wet Steel Welds. Metallurgical and Materials Engineering Department, Colorado School of Mines, Golden, Colorado, EUA, Dissertation, 128f , 1999.

ROWE, M. D. e LIU, S. Recent Development in Underwater Wet Welding. Science and Technology of Welding and Joining, Vol. 6, No. 6. pp 387-396, 2001.

ROWE M. D., LIU S. and REYNOLDS T. J. The Effect of Ferro-Alloy additions and Depth on the Quality of Underwater Wet Welds. Welding Journal, August 2002, pp. 156-S-166-S, 2002.

SUGA, Y. and HASUI, A. On Formation of Porosity in Underwater Weld Metal. IIW Doc. IX – 1388-86, Cambridge, 1986.

APPENDIX A: The Gravimetric Method for Porosity Quantification

The technique used to evaluate porosity is described in the ASTM standard B 311-93: "Test Method for Powder Metallurgy Materials Containing Less than Two Percent Porosity". This method is based on water displacement. The standard is recommended for specimens with less than two percent porosity. The basic principles of the method and the precision of the scale used make it an adequate technique to measure even larger porosity as it was found in this research. The balance used was a high sensitivity Mettler Toledo AB204. In this technique, porosity is calculated from the difference between the densities of the base metal and of the weld metal.

The process starts with the preparation of the steel samples for wet welding. A steel bar of ½ x 1 x 8 inches (12.7 x 25.4 x 200 mm) is sectioned in 4 pieces of approximately ½ x 1 x 2 inches (12.7 x 25.4 x 50 mm), as shown in Figure A3. Clear identification of the two pieces is required using different number or letters on the opposite side of the weld or on the lateral side of the plate. Two pieces of the base metal are weighted in dry conditions (W_{BMdry}) and weight again suspended and completely submerged into water (W_{BMsub}), using the parts showed in Figure A4, as shown in Figure A5. With these two weights and the water density (which varies with temperature), the volume (V_{BM}) and the density (ρ_{BM}) of the base metal can be calculated, as shown in Equations A1 and A2.

$$V_{BM} = \frac{W_{BMdry} - W_{BMsub}}{\rho_{H_2O}} \qquad \text{Eq. A1}$$

$$\rho_{BM} = \frac{W_{BMdry}}{V_{BM}} \qquad \text{Eq. A2}$$

Once the weld has been deposited on the four pieces, the base metal is submerged in liquid nitrogen and the weld is broken in four pieces. The two indentified pieces with the weld bead are weighted in dry conditions ($W_{BM+WMdry}$) and submerged in water ($W_{BM+WMsub}$), using the same device showed in Figure A5. With these two weights and the water density, the volume (V_{BM+WM}) and the density (ρ_{BM+WM}) of the base metal with the weld metal can be calculated, with Equations A3 and A4.

$$V_{BM+WM} = \frac{W_{BM+WMdry} - W_{BM+WMsub}}{\rho_{H_2O}} \qquad \text{Eq. A3}$$

$$\rho_{BM+WM} = \frac{W_{BM+WMdry}}{V_{BM+WM}} \qquad \text{Eq. A4}$$

Considering that there is one case where the weld presents zero penetration and in a second case the weld presents higher penetration, there are two different approaches to calculate the porosity in the weld metal, as described below.

A.1. Porosity calculation for zero weld penetration

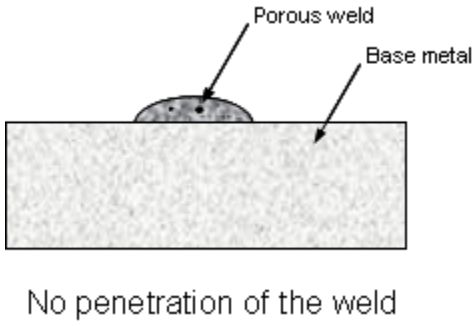

Figure A.1. Weld with no penetration.

The volume of the weld metal (V_{WM}) can be calculated using Equation A5. The weight of the weld metal (W_{WM}) can be calculated by subtracting the weight of the base metal from the weight of the base metal with the weld metal, Equation A6.

$$V_{WM} = V_{BM+WM} - V_{BM} \qquad \text{Eq. A5}$$

$$W_{WM} = W_{BM+WM} - W_{BM} \qquad \text{Eq. A6}$$

Using the equations A5 and A6, the density of the weld metal (ρ_{WM}) can be calculated with Equation A7.

$$\rho_{WM} = \frac{W_{WM}}{V_{WM}} \qquad \text{Eq. A7}$$

The equivalent weld metal volume associate (V_{EWM}) considering that the weld metal is free of pores is calculated with Equation A8.

$$V_{EWM} = \frac{W_{WM}}{\rho_{BM}} \qquad \text{Eq. A8}$$

So, with the volume of the weld metal (V_{WM}) and the volume associate (V_{EWM}), the volume of pores (V_P) can be calculated as shown in Equation A9.

$$V_P = V_{WM} - V_A \qquad \text{Eq. A9}$$

Based on the volume of the pores (V_P) and on the volume of the weld metal (V_{WM}), porosity is calculated using Equation A10, considering that there are no pores in the base metal.

$$Porosity(\%) = \frac{V_P}{V_{WM}} \times 100 \qquad \text{Eq. A10}$$

A.2. Porosity calculation for deeper weld penetration

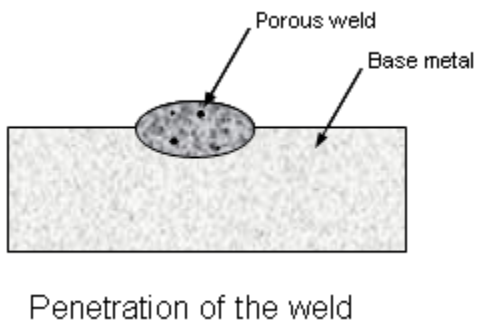

Figure A.2. Weld with deeper penetration.

After calculating the density of the base metal (Eq. A2) and the density of the base metal with the weld metal (Eq. A4), the difference between these two values should be zero if there are no pores in the weld metal or different of zero when there is porosity on the weld metal. The difference between these two values of the density ($\Delta\rho$), is given by Equation A11.

$$\Delta\rho = \rho_{BM} - \rho_{BM+WM} \qquad \text{Eq. A11}$$

The volume associated to the density difference is the volume of pores (V_P) in the weld metal and it is calculated as shown in Equation A12.

$$V_P = \frac{\Delta\rho}{\rho_{BM}} \qquad \text{Eq. A12}$$

Equation A13 is for the calculation of the weld metal volume (V_{WM}), which is the cross sectional area of the weld bead (A_W) times the length of the weld segment (L_W).

$$V_{WM} = A_W \cdot L_W \qquad \text{Eq. A13}$$

Then, porosity is given in percentage by Equation A14, which is a combination of equations A12 and A13.

$$Porosity(\%) = \frac{V_P}{V_{WM}} \times 100 \qquad \text{Eq. A14}$$

For both cases, weighting the samples into water requires special care to remove any small bubble adhered to the surface of the sample, as well as to the surface of the submerged hanger.

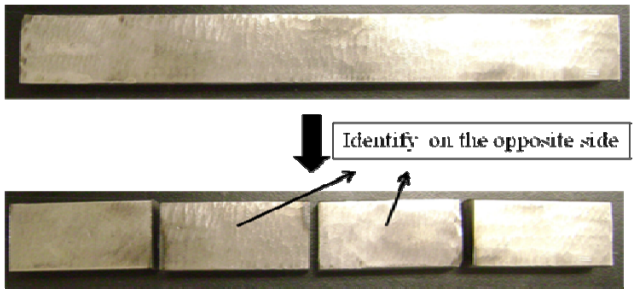

Figure A3. Base metal preparation.

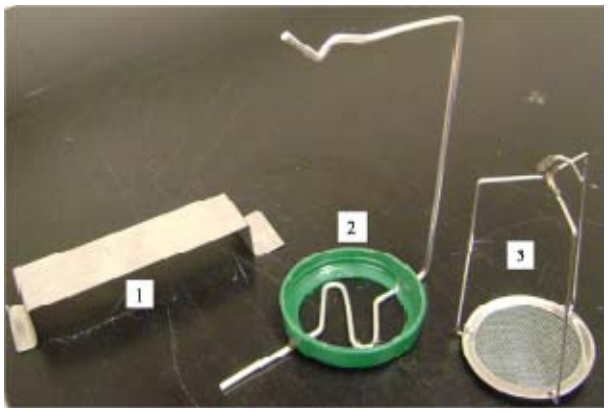

Figure A4. Equipment used to weight sample suspended.
1 – Support for the beaker; 2 – Support for the hanger; 3 – Hanger.

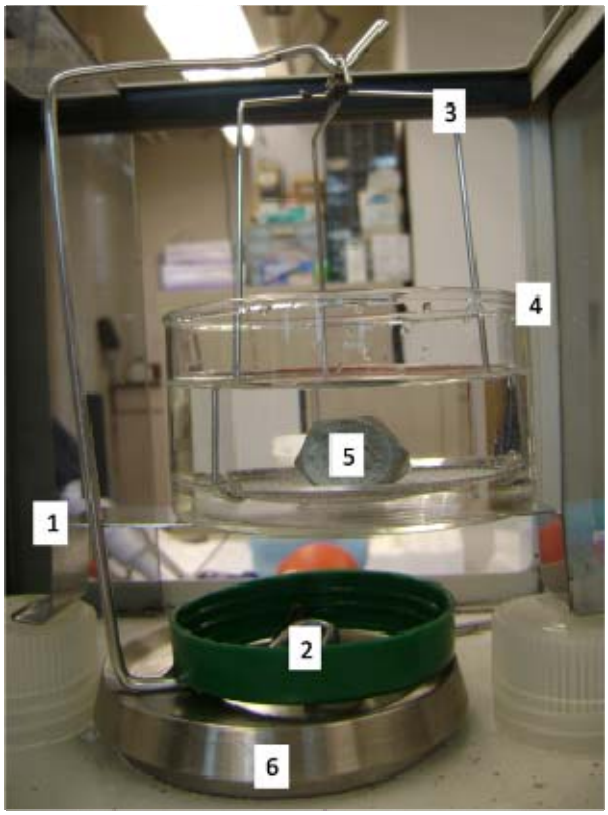

Figure A5. Device used to measure the wet weight.
1 – Support for the beaker; 2 – Support for the hanger; 3 – Hanger; 4 – Beaker; 5 – Sample; 6 – Balance pan.

APPENDIX B: Minerals Particle Size Distribution Used to Extrusion

One difference between the electrodes extruded by Devasco International and by CSM was the particle size distribution of the minerals used. Basically Devasco International used finer minerals than those used at CSM. Flux coatings with ingredients that had finer particle size distribution exhibited better extrudability. Flux coatings with ingredients with coarser particle size distribution exhibited higher welding voltage and less short circuiting transfer. The next figures will show a comparison between each mineral used by Devasco, International and by CSM in the electrode extrusion.

Table B1 shows the relation between the mesh number and the size of the mesh used to sieve the minerals.

Table B1. Relation between the mesh number used and the size of the mesh.

Mesh Number	Spacing, mm
65	230µ
100	150µ
150	100µ
200	75µ
325	45µ
400	38µ

As shown in Table 1, rutile is the main ingredient in the flux with 41.8 and 39% in formula "Wet 1" and "Wet 2", respectively. Figure B1 presets a comparison of the particle size distribution of rutile used by CSM and Devasco, International. As one can see in Fig B1, 30% of the rutile used by DEVASCO was retained in a finer mesh number 325.

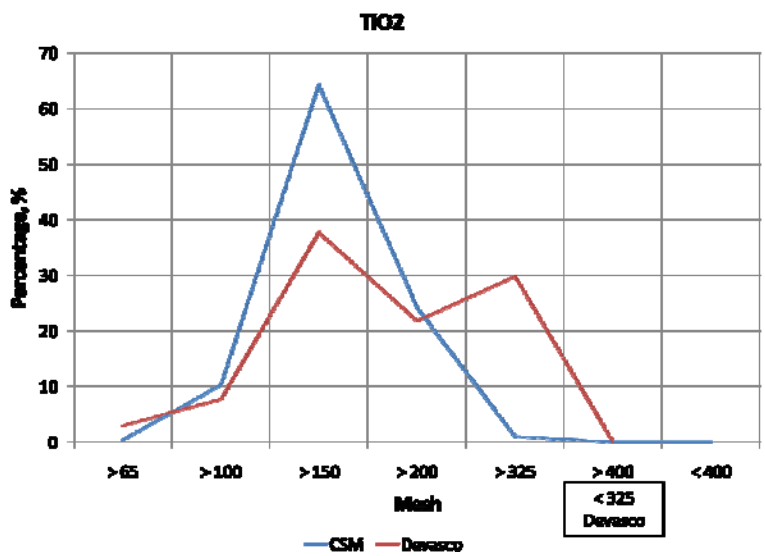

Figure B1. Particle size comparison of TiO_2.

Feldspar, mica and silica minerals used by CSM are coarser than the ones used by Devasco, International as clearly shown in Figure B2, B3, and B4.

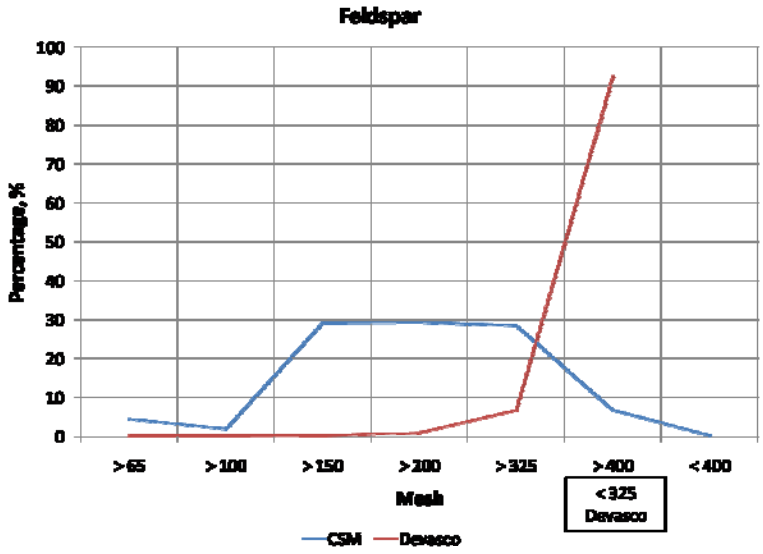

Figure B2. Particle size comparison of feldspar.

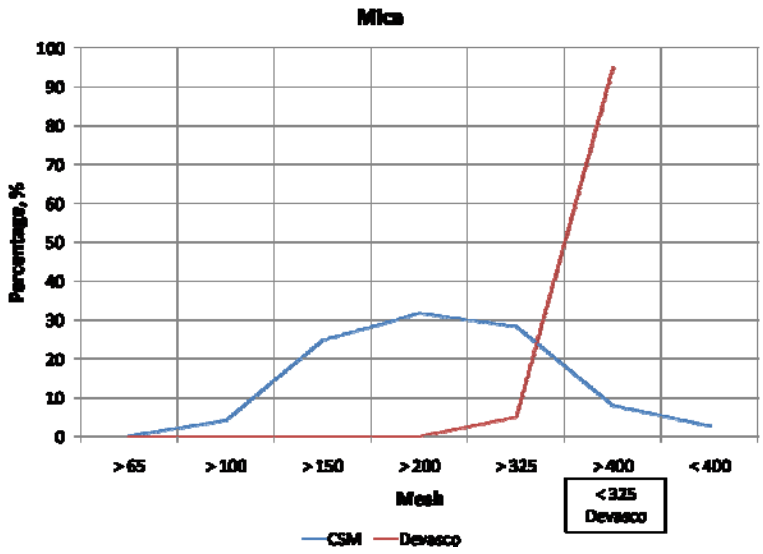

Figure B3. Particle size comparison of mica.

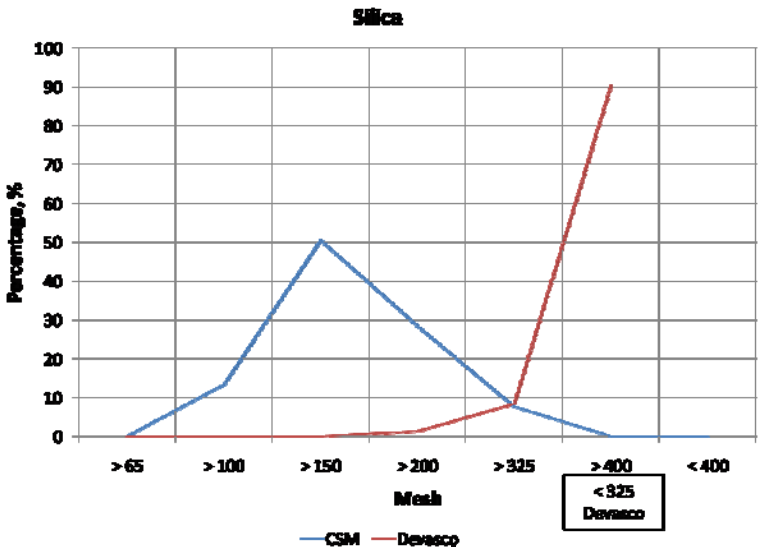

Figure B4. Particle size comparison of silica.

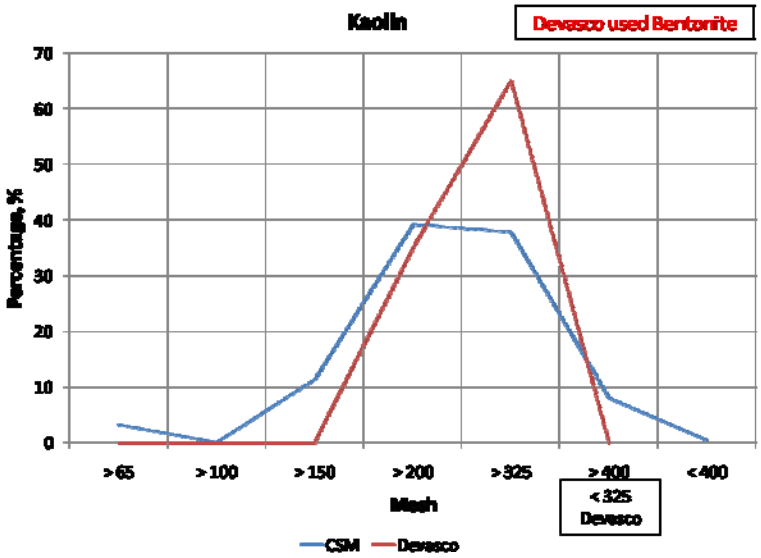

Figure B5. Particle size comparison of kaolin.

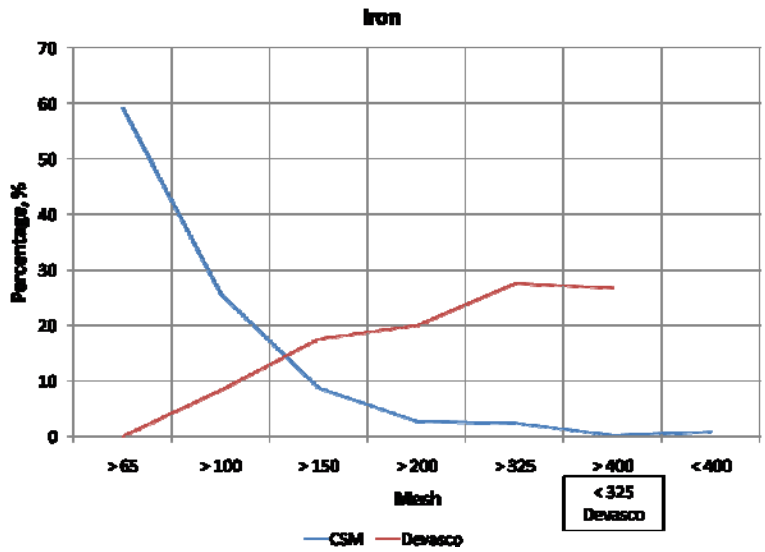

Figure B6. Particle size comparison of iron.

Marflux and Ferro-boron are the only minerals used by CSM with finer particle size than the one used by Devasco, International.

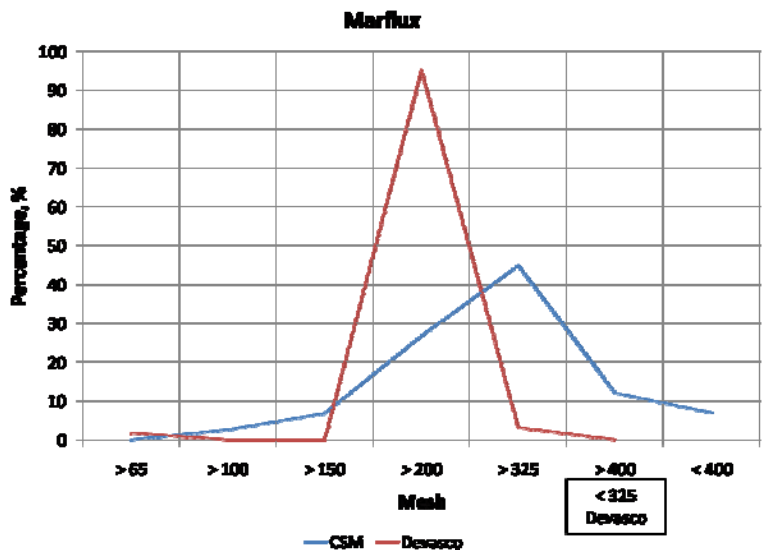

Figure B7. Particle size comparison of marflux.

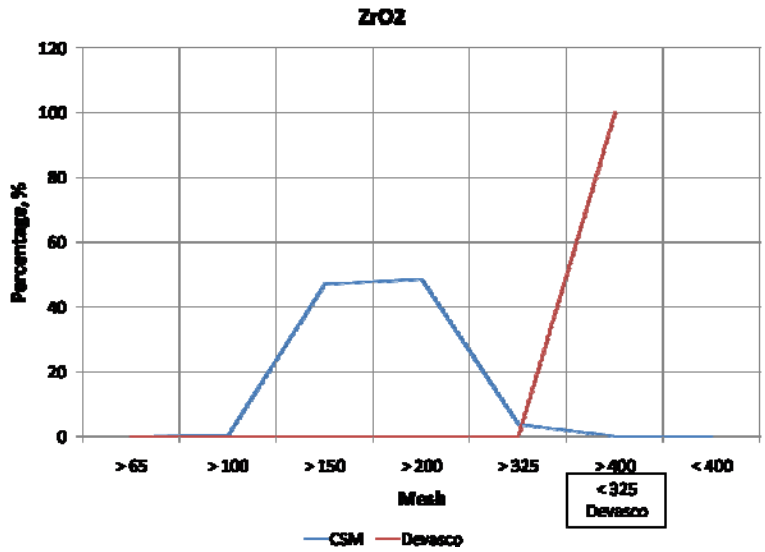

Figure B8. Particle size comparison of ZrO_2.

Ferro-manganese is an important alloying addition to the flux coating with 16%. In this case 50% and 13% of the Fe-Mn used by Devasco, International and CSM was retained in mesh number 200, respectively.

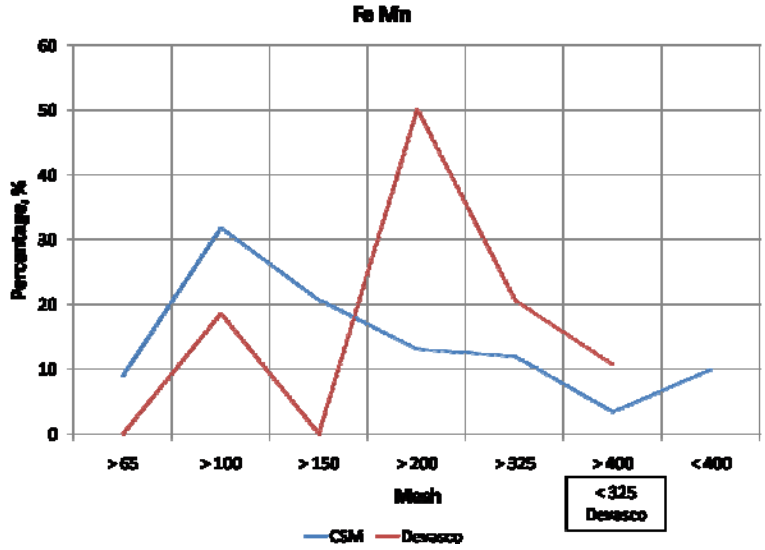

Figure B9. Particle size comparison of Fe-Mn.

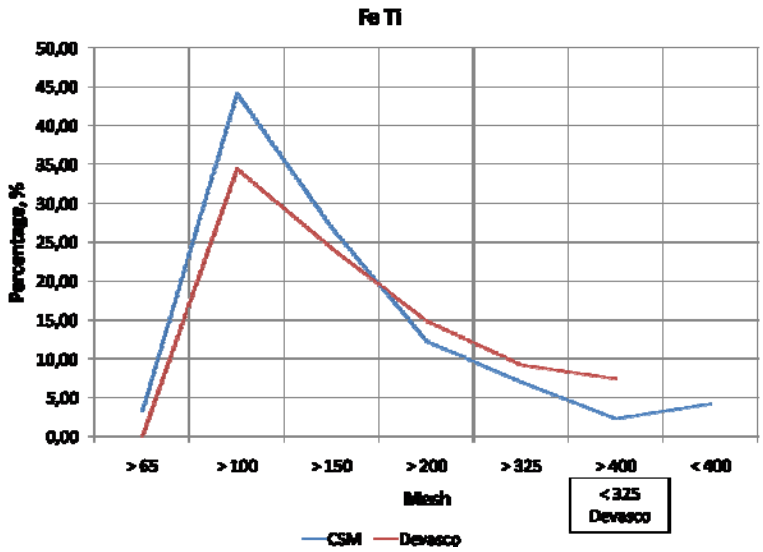

Figure B10. Particle size comparison of Fe-Ti.

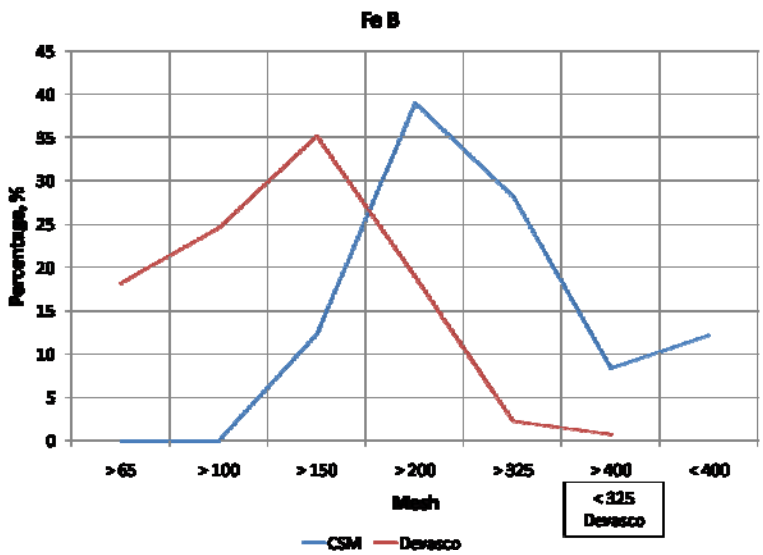

Figure B11. Particle size comparison of Fe-B.